

# LADDER: Language-Driven Slice Discovery and Error Rectification in Vision Classifiers

Anonymous ACL submission

## Abstract

Slice discovery refers to identifying systematic biases in the mistakes of pre-trained vision models. Current slice discovery methods in computer vision rely on converting input images into sets of attributes and then testing hypotheses about configurations of these pre-computed attributes associated with elevated error patterns. However, such methods face several limitations: 1) they are restricted by the predefined attribute bank; 2) they lack the *common sense* reasoning and domain-specific knowledge often required for specialized fields *e.g.*, radiology; 3) at best, they can only identify biases in image attributes while overlooking those introduced during preprocessing or data preparation. We hypothesize that bias-inducing variables leave traces in the form of language (*e.g.*, logs), which can be captured as unstructured text. Thus, we introduce LADDER, which leverages the reasoning capabilities and latent domain knowledge of Large Language Models (LLMs) to generate hypotheses about these mistakes. Specifically, we project the internal activations of a pre-trained model into text using a retrieval approach and prompt the LLM to propose potential bias hypotheses. To detect biases from preprocessing pipelines, we convert the preprocessing data into text and prompt the LLM. Finally, LADDER generates pseudo-labels for each identified bias, thereby mitigating all biases without requiring expensive attribute annotations. Rigorous evaluations on 3 natural and 3 medical imaging datasets, 200+ classifiers, and 4 LLMs with varied architectures and pretraining strategies – demonstrate that LADDER consistently outperforms current methods. Code is available: <https://github.com/anonymous-vision/ACL>.

## 1 Introduction

Error slices are data subsets on which vision classifiers systematically fail. Discovering such slices is critical for improving model robustness. Identifying such slices is challenging in vision classifiers where biases are pervasive and can be traced through textual artifacts such as image captions, metadata, and medical imaging headers *e.g.*, DICOMs. However, their unstructured nature makes manual analysis impractical. Natural language, with its inherent flexibility, offers a powerful tool for capturing subtle biases beyond predefined attribute sets. LLMs, equipped with advanced reasoning capabilities and latent domain knowledge, excel at analyzing such free-form text to detect complex relationships and domain-specific biases. However, existing slice discovery methods often rely on predefined attribute banks or unsupervised clustering, both of which lack the reasoning ability to identify nuanced and domain-specific biases. This paper proposes LADDER, that leverages LLMs to systematically identify and mitigate error slices in vision classifiers by analyzing captions, metadata, and beyond – without relying on fixed attribute sets or clustering methods.

Prior slice discovery methods *e.g.*, DrML (Zhang et al., 2023) use text encoders to mitigate biases in CLIP by closing the modality gap through cross-modal transfer, which limits their applicability to non-multimodal models. Plus, DrML relies on user-defined prompts with fixed attribute sets, introducing human bias into the mitigation process. Similarly, Facts (Yenamandra et al., 2023) amplifies the spuriousness in the initial training stage by setting large weight decay, deviating from standard supervised learning practices. Methods like



Figure 1: Synthetic dataset containing Class 0 images consistently with a yellow box to the left of a red box, while Class 1 images have boxes placed randomly. Captions encode the spatial bias, used by LADDER for slice discovery.

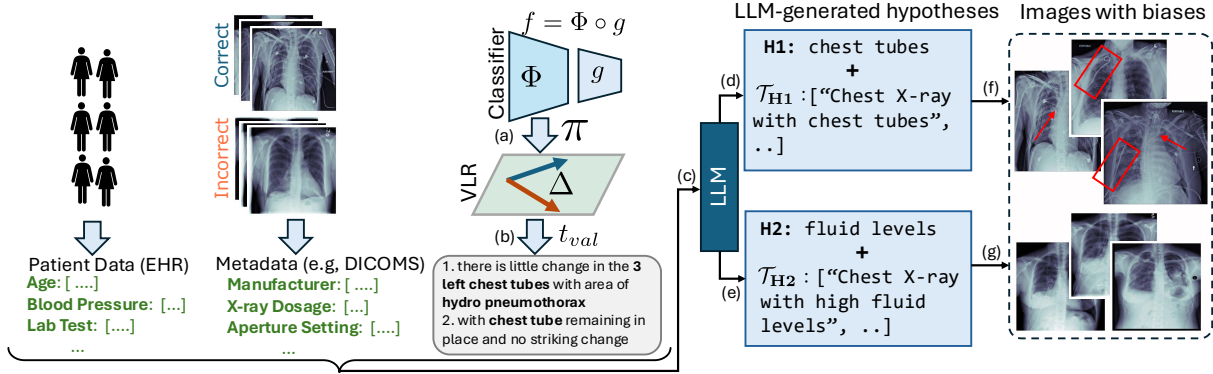


Figure 2: Schematic of LADDER. (a): Projection ( $\pi$ ) of model representation ( $\Phi$ ) to VLR space. (b): Retrieval of topK sentences based on the image embeddings difference ( $\Delta$ ) of correct and incorrect groups in VLR space. (c): LLM is invoked with topK sentences/other metadata. (d-e): LLM generated hypotheses ( $\{\mathcal{H}, \mathcal{T}\}$ ). (f-g): Finding the clusters faithful to the hypotheses. In red, we highlight the chest tubes (ground truth bias for NIH) in this example.

Domino (Eyuboglu et al., 2022) and Facts discover slices by clustering samples with similar attributes within the vision-language representation (VLR) space. However, the slices often exhibit semantic inconsistencies – attributes within slices lack coherence, leading to unreliable interpretations of model errors. PRIME (Rezaei et al., 2023) relies on expensive tagging models, limited to detecting the presence/absence of a fixed set of attributes. All these methods lack the reasoning capabilities and domain knowledge required to capture complex error patterns, limiting their effectiveness in specialized tasks. Also, their dependence on pre-existing semantic labels (e.g., visual tags) hinders the detection of biases in the metadata or domain-specific fields such as DICOM headers.

Prior mitigation methods (Sagawa et al., 2020; Liu et al., 2021; Kirichenko et al., 2022) rely on expensive and incomplete attributes. While they improve worst group accuracy (WGA), they amplify errors in other groups (Li et al., 2023b). Although Li et al. (2023b) addresses errors across multiple biases, it assumes prior knowledge of the number and types of biases to design specific data augmentations. This reveals a critical gap: the need for an automated method to discover and mitigate multiple biases without prior knowledge/annotations.

This paper proposes LADDER with the following contributions: **1. Using language for error slice discovery:** LADDER uses image captions/radiology reports to retrieve sentences indicative of model errors, utilizing the flexibility of natural language to capture deeper insights beyond the simple presence or absence of attributes, unlike tagging models. **2. Using LLMs’ reasoning capabilities and latent domain knowledge:** To identify biases, LADDER

leverages LLMs’ advanced reasoning to generate testable hypotheses from these sentences, unlike traditional methods. For instance, in a synthetic dataset (Appendix A.11), where Class 0 images consistently feature a yellow box to the left of a red box (Fig 1), the classifier exhibits poor performance on test data without this bias. LADDER correctly identifies this reliance on spatial positioning by analyzing textual descriptions through LLM (Fig 11). Note, LLM in LADDER processes only text inputs without images (total cost of  $\sim$ \$28). In medical images, LADDER uses LLMs’ domain knowledge to identify fine-grained biases, including disease subtypes and pathological patterns. **3. Slice discovery from any off-the-shelf model:** It detects slices from any supervised model, regardless of architecture/pretraining, overcoming specific training requirements of Facts and DrML. **4. Detecting biases beyond captions:** LADDER uses LLM to analyze metadata, such as Electronic Health Records (EHR) or DICOM headers, discovering biases beyond captions. **5. Mitigating multiple biases w/o any annotation:** LADDER mitigates biases by generating pseudo-labels for each hypothesis and fine-tuning the classifier’s linear head through attribute rebalancing. By ensembling debiased model predictions, LADDER corrects multiple biases without requiring attribute annotations/prior knowledge of their number and type. **Additionally,** we explore the use of instruction-tuning models (e.g., LLaVA) in applicable domains to reduce LADDER’s reliance on captions. Rigorous evaluations on 6 datasets with 200+ classifiers and 4 LLMs across architectures and pretraining strategies show that LADDER outperforms slice discovery and mitigation baselines.

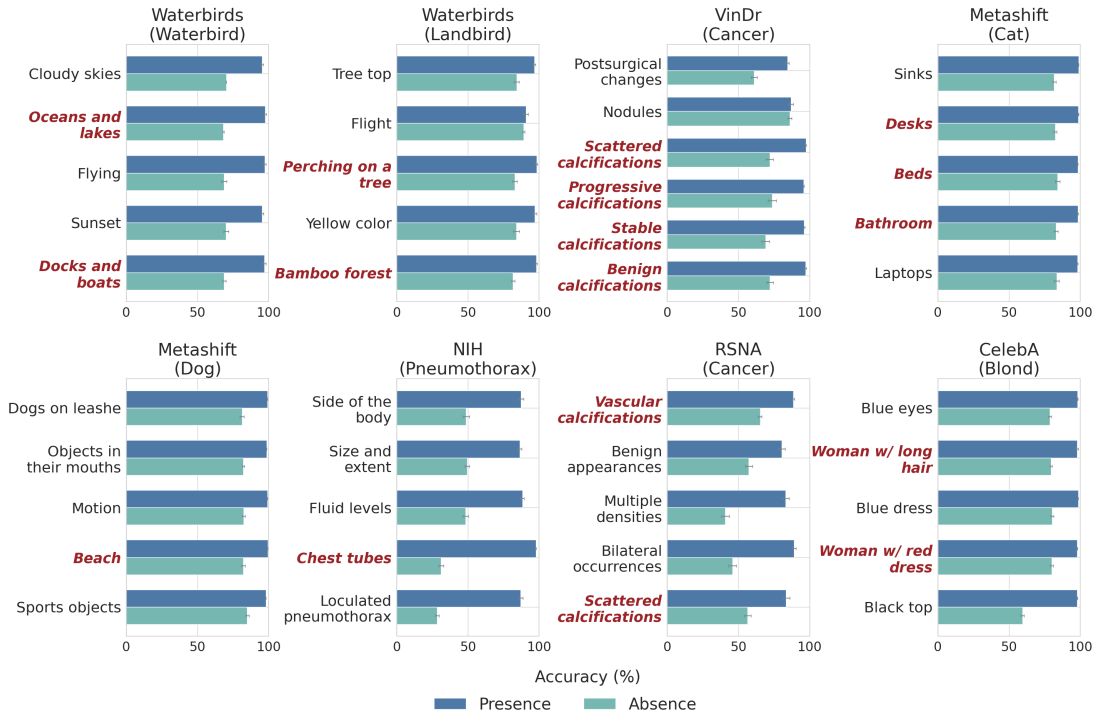


Figure 3: Bias identification by LADDER in RN Sup IN1k classifier. Each panel shows the classifier’s performance for a specific dataset (RSNA) and class label (Cancer) when biased attributes in the identified hypotheses are present/absent. Hypotheses indicative of ground truth biases (*e.g.*, water for waterbirds) are shown in red.

## 2 Related Work

**Slice discovery.** Initial methods (d’Eon et al., 2022; Sohoni et al., 2020; Kim et al., 2019; Singla et al., 2021) on slice discovery utilize dimensionality reduction, lacking comprehensive evaluation. Recent methods *e.g.*, Domino (Eyuboglu et al., 2022) projects data into VLR space, identifies slices via a mixture model, and captions them. Facts (Yenamandra et al., 2023) amplifies spurious correlations in the initial training phase by increasing weight decay and discovering slices in VLR space. Both approaches compromise visual semantics, resulting in attribute inconsistencies within slices. DrML (Zhang et al., 2023) probes only CLIP-based classifiers using modality gap geometry and user-defined prompts, introducing potential human biases. Also, Facts and DrML are restricted to specific training setups, limiting generalizability to standard ERM classifiers. PRIME (Rezaei et al., 2023) uses expensive tagging models to discover attributes for slice discovery. HiBug (Chen et al., 2024a) prompts LLM to suggest biases for model errors without any textual context from the data. Thus, it results in superficial keyword-based attributes derived purely from general user prompts, lacking the deeper contextual grounding needed for bias detection. Recently, OpenBias (D’Incà et al.,

2024) detects biases in T2I models via LLM-driven keyword queries but is not designed for posthoc classifier error analysis. B2T (Kim et al., 2024) extracts keywords from captions. All these methods are limited by incomplete tags or keyword-based attributes and lack reasoning or latent *domain knowledge*, essential in fields *e.g.*, radiology. **Bias mitigation.** Mitigation methods *e.g.*, GroupDRO (Sagawa et al., 2020) optimizes for worst-performing groups, while JTT (Liu et al., 2021) reweights minority groups. DFR (Kirichenko et al., 2022) retrains the final layer using a balanced validation set. All of them require group annotations and focus on mitigating errors in the worst-performing group, amplifying errors in other subgroups. Li et al. (2023b) mitigates multiple biases using an ensemble-based approach but relies on predefined bias types, which limits its adaptability to unknown biases. LADDER overcomes all these limitations. For discovery, LADDER incorporates the *domain knowledge* of LLMs, reason about model errors, and generates hypotheses identifying biases from any pre-trained model without external attributes, unlike existing methods. For mitigation, LADDER leverages pseudo-labels for each bias to finetune the classifier’s last layer – without any group annotations, predefined bias types, or human intervention.

### 3 Method

Assume the classifier  $f = g \circ \Phi$  is trained using ERM to predict the labels  $\mathcal{Y}$  from the images  $\mathcal{X}$ , where  $\Phi$  and  $g$  are the representation and classification head, respectively.  $\{\Psi^I, \Psi^T\}$  denote the image and text encoders of the joint VLR space. For a set of images  $\mathcal{X}_Y$  of a class  $Y \in \mathcal{Y}$ , LADDER identifies error slices where  $f$  underperforms and mitigates it. Throughout the paper,  $\langle \cdot, \cdot \rangle$  denotes the dot product to estimate the similarity between two representations. Fig. 2 shows the schematic of LADDER. We do not rely on sample-specific paired annotations, human-generated prompts, or prior knowledge of bias types or their numbers. We utilize a text corpus  $t_{val}$  from radiology reports or image captions from the validation dataset to discover and mitigate errors. **Error slice.** An error slice for a class  $Y$  includes subsets  $\mathcal{X}_Y$  where the model performs significantly worse than its overall performance on the entire class  $Y$ , formally defined as:  $\mathbb{S}_Y = \{\mathcal{S}_{Y,-attr} \subseteq \mathcal{X}_Y | e(\mathcal{S}_{Y,-attr}) \gg e(\mathcal{X}_Y), \exists attr\}$ , where  $e(\cdot)$  is the error rate on the specific data subset and  $\mathcal{S}_{Y,-attr}$  denotes the subset of  $\mathcal{X}_Y$  without the attribute  $attr$ . Alternatively,  $f$  is biased on the attribute  $attr$ , resulting in better performance on the subpopulation with  $attr$  e.g., error rate in pneumothorax patients w/o chest tubes is higher than overall pneumothorax patients (Docquier and Rapoport, 2012).

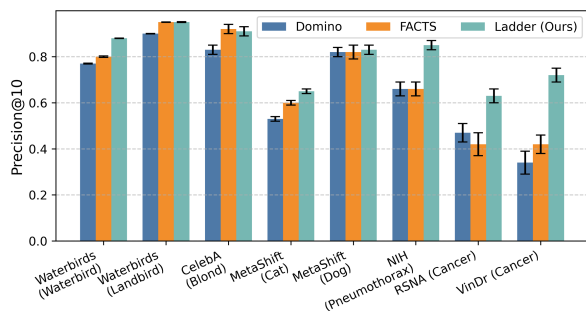


Figure 4: Precision@10 for CNN models ( $f$ ) quantifying slice discovery. LADDER outperforms the baselines, especially for medical imaging datasets.

#### 3.1 Retrieving Sentences Indicative of Biases

First, for a particular class, LADDER retrieves the sentences that describe the visual attributes contributing to correct classifications but missing in misclassified ones, leading to model errors. Following Moayeri et al. (2023), it learns a projection function  $\pi : \Phi \rightarrow \Psi^I$  (Appendix A.4) to align the representation of the classifier,  $\Phi$ , with the image representation  $\Psi^I$  of the VLR space.

Then, for a class label  $Y$ , we estimate the difference in mean of the projected representations of the correct and misclassified samples as  $\Delta^I = \mathbb{E}_{X,Y|f(X)=Y}[\pi(\Phi(X))] - \mathbb{E}_{X,Y|f(X) \neq Y}[\pi(\Phi(X))]$ . Assuming the mean representations preserve semantics, this difference captures key attributes contributing to correct classifications but are poorly captured or misrepresented in misclassified ones. Denoting the text embedding of  $t_{val}$  as  $\Psi^T(t_{val})$ , we retrieve the topK sentences as:  $\text{topK} = \mathcal{R}(\langle \Delta^I, \Psi^T(t_{val}) \rangle, t_{val})$ , where  $\mathcal{R}$  is a retrieval function retrieving topK sentences from the text corpus having the highest similarity score with the mean difference of the projected image representations. Next, the LLM analyzes the sentences and constructs hypotheses to find error slices.

#### 3.2 Discovering Error Slices via LLM

**Generating hypothesis.** To form the set of hypotheses, LADDER invokes an LLM with the topK sentences. Formally,  $\{\mathcal{H}, \mathcal{T}\} = \text{LLM}(\text{topK})$ , where  $\mathcal{H}$  is a set of hypotheses with attributes that  $f$  may be biased and  $\mathcal{T}$  is a set of sentences to be used to test each hypothesis.  $f$  underperforms on the subpopulation without the attributes in  $\mathcal{H}$ . Each hypothesis  $H \in \mathcal{H}$  is paired with  $\mathcal{T}_H \in \mathcal{T}$ , a set of sentences that provide diverse contextual descriptions of the hypothesis-specific attribute as it appears in various images. Representations of images with the attribute specified in  $H$ , are highly similar to the mean text embedding of  $\mathcal{T}_H$ . Refer to Appendix A.7 for the prompt used by LLM to generate the hypothesis. **Identifying error slices.** For each hypothesis  $H \in \mathcal{H}$ , we first compute the mean embedding of the set of sentences  $\mathcal{T}_H$  as  $\Psi^T(\mathcal{T}_H) = \frac{1}{|\mathcal{T}_H|} \sum_{t \in \mathcal{T}_H} \Psi^T(t)$ . For an image  $X \in \mathcal{X}_Y$ , we obtain the projected representation  $\pi(\Phi(X))$  in VLR space and compute the similarity score,  $s_H(X) = \langle \pi(\Phi(X)), \Psi^T(\mathcal{T}_H) \rangle$ . Finally, for a class label  $Y$ , we retrieve images with similarity scores below a threshold  $\tau$  as  $\mathcal{S}_{Y,-H} = \{X \in \mathcal{X}_Y | s_H(X) < \tau\}$ . The hypothesis  $H$  fails in these images as they lack the attribute specified in the  $H$ . The subset  $\mathcal{S}_{Y,-H}$  may be a potential error slice if the error  $e(\mathcal{S}_{Y,-H})$  is greater than  $\mathcal{X}_Y$ . Formally,  $\hat{\mathbb{S}}_Y$ , the predicted slice for a class  $Y$  is:  $\hat{\mathbb{S}}_Y = \{\mathcal{S}_{Y,-H} \subseteq \mathcal{X}_Y | e(\mathcal{S}_{Y,-H}) \gg e(\mathcal{X}_Y), \exists H \in \mathcal{H}\}$

#### 3.3 Mitigate Multi-bias w/o Annotation

For the attributes linked to a hypothesis, LADDER treats  $s_H$  as a logit and converts it to a probability. If the probability exceeds a threshold (0.5 in all

experiments), LADDER assigns a pseudo-label 1 to the attribute and 0 otherwise. Thus, it generates pseudo-labels for all relevant attributes, enabling error mitigation without annotations. To do so, LADDER adopts an ensemble-based strategy. Following DFR, we create a balanced dataset from a held-out validation set, for each pseudo-labeled attribute per hypothesis. We then fine-tune the classification head  $g$  using this balanced dataset, producing a debiased model per hypothesis. During inference, we again compute the similarity score  $s_H$  for all hypotheses and select the classifier head  $g_{H^*}$  associated with the hypothesis having maximum similarity:  $H^* = \arg \max_{H \in \mathcal{H}} s_H(X)$ .

## 4 Experiments

We perform experiments to answer the research questions: **RQ1.** How does LADDER perform in discovering error slices compared to baselines? **RQ2.** How does LADDER leverage reasoning and latent domain knowledge of LLMs for slice discovery? **RQ3.** How does LADDER discover biased attributes with different architectures and pre-training methods? **RQ4.** How does LADDER mitigate biases using the discovered attributes? **RQ5.** Can LADDER operate w/o captions? **RQ6.** Can LADDER detect biases beyond captions/reports?

**Datasets.** We evaluate LADDER on 6 datasets (Appendix A.1 for details): 1) **Waterbirds** (Wah et al., 2011): bird classification where background correlates with bird type. 2) **CelebA** (Liu et al., 2018): blond hair classification with gender as a spurious feature. 3) **MetaShift**: cat vs. dog classification with background correlation. 4) **NIH Chest-X-ray (CXR)** (Wang et al., 2017): pneumothorax detection with chest tubes as a shortcut (Docquier and Rapoport, 2012). 5) **RSNA-Mammo** and 6) **VinDr-Mammo** (Nguyen et al., 2023): breast cancer and abnormality detection from mammograms, with calcifications as a shortcut (Wen et al., 2024).

**Experimental details.** For natural images and CXRs, we use an ImageNet1k (IN1k)-initialized ResNet50 (RN Sup IN1k) as the model  $f$  that LADDER aims to probe, trained with a standard supervised loss. For mammograms, we use EfficientNet-B5 (EN-B5) as  $f$ . For the text corpus ( $t_{val}$ ), we use BLIP-captioner (Li et al., 2022), radiology reports from MIMIC-CXR (Johnson et al., 2019) and the radiology texts from MammoFActOR (Ghosh et al., 2024) for natural images, CXRs and mammograms, respectively. For VLR

space ( $\{\Psi^I, \Psi^T\}$ ), we use CLIP (Radford et al., 2021), CXR-CLIP (You et al., 2023), and Mammo-CLIP (Ghosh et al., 2024) for natural images, CXR and mammograms, respectively. We use 200 and 100 sentences as topK for natural and medical images (CXR and mammo). We use GPT-4o (Wu et al., 2024) as the LLM. Error slices are defined as subsets where the error rate exceeds the overall class error by at least 10%. Refer to Appendix A.10 for further experimental details. All reported results are obtained from experiments conducted over 3 random seeds.

**Baselines.** For slice discovery, we compare LADDER with Domino and Facts (Appendix A.2). For mitigation, we compare with the baselines, including ERM (Vapnik, 1999), GroupDRO (Sagawa et al., 2020), JTT (Liu et al., 2021), DFR (Guo et al., 2019), CVaRDRO (Duchi and Namkoong, 2021) and LfF (Nam et al., 2020) (Appendix A.3).

**Evaluation metrics.** We use Precision@10 (Appendix A.5) (Eyuboglu et al., 2022) to evaluate the slice discovery methods and the CLIP score (Kim et al., 2024) to quantify the effect of biased attributes. For mitigation, we report Worst Group Accuracy (WGA) for mitigation for natural images. We report mean AUROC and WGA for medical images, where WGA refers to model performance on pneumothorax patients w/o chest tubes (NIH) and cancer or abnormal patients w/o calcifications (RSNA & VinDr-Mammo).

## 5 Results

**RQ1: Comparison of LADDER with slice discovery baselines.** Following (Eyuboglu et al., 2022; Yenamandra et al., 2023), Fig. 4 compares the Precision@10 of different slice discovery methods for CNN models (EN-B5 for mammograms & RN Sup IN1k for others). For medical images, LADDER achieves a substantial **50%** improvement over the baselines. Refer to Fig. 12 in Appendix A.12.1 for WGA evaluation using the slices discovered from Domino, Facts, and LADDER with our ensemble-based mitigation strategy. In all the experiments, LADDER outperforms the baselines. Facts and Domino cluster the images by projecting them directly into VLR space, often leading to incoherent slices. In contrast, LADDER first projects the model’s representation into the VLR space, preserving the nuanced semantics of the classifier features. Instead of relying solely on unsupervised clustering, it leverages the reasoning capabilities of LLMs

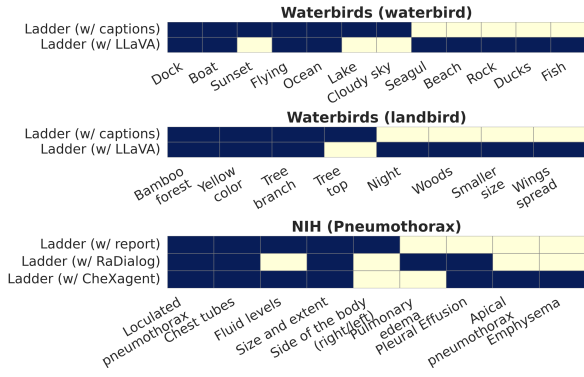


Figure 5: Biased attributes detected by LADDER w/ captions and w/ instruction-tuned models (w/o captions). Bright/light colors show presence/absence of attributes

and signals from the captions/radiology reports to identify the coherent-biased attributes within the discovered slices. Next, we assign pseudo-labels to the attributes using similarity scores ( $s_H(X)$ ). The coherent slices produced by LADDER ensure that the pseudo-labeling process is more accurate than the baselines leading to superior bias mitigation performance (Appendix A.12.1).

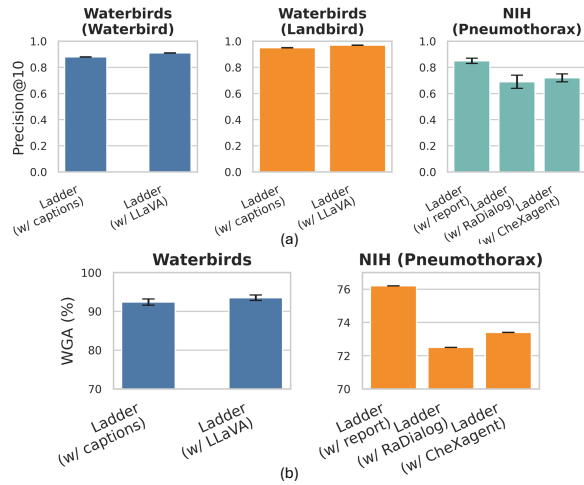


Figure 6: (a) Precision@10 for slice discovery and (b) WGA for bias mitigation using LADDER w/ captions vs. instruction-tuned models.

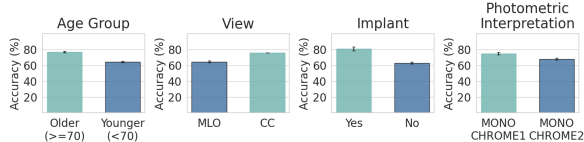


Figure 7: LADDER detects biases beyond reports, identifying biases from metadata (age, view and implant) and DICOM headers (Photometric interpretation).

**RQ2. Leveraging LLM’s reasoning and domain knowledge for bias discovery.** Fig. 8 displays the sentences retrieved by LADDER indicat-

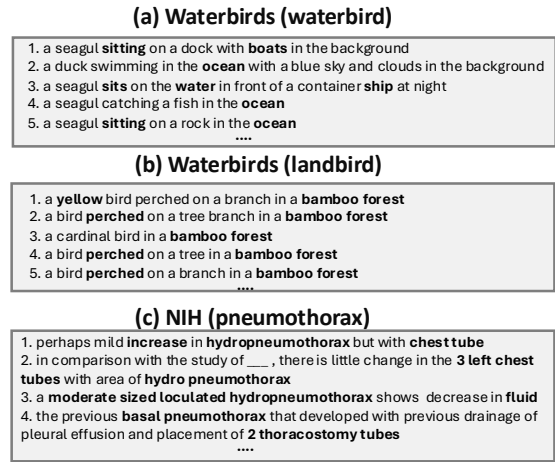


Figure 8: Sentences retrieved by LADDER in Sec. 3.1 encoding model biases (in bold) for LLM to analyze. Each panel denotes a class label of a specific dataset.

ing the different model biases. Fig. 3 shows the biased attributes discovered by LADDER. The presence of these attributes correlates with  $f$ 's performance, while their absence results in error slices where  $f$ 's performance drops. Recall, LADDER uses LLM to generate hypotheses from the sentences, indicative of biases. The similarity score ( $s_H(X)$ ) tests these hypotheses to validate if the absence of specific attributes linked to each hypothesis results in a drop in  $f$ 's performance. For *e.g.*, waterbirds flying vs. not flying achieve 97.3% vs. 68.6% accuracy. In NIH, pneumothorax patients with and without chest tubes achieve an accuracy of ~98%, compared to 31%. For all tasks, LADDER effectively detects ground truth biases. In the Waterbirds dataset, LADDER identifies diverse water-related biases such as boat and lake. Also, Fig.3 reports that LADDER identifies domain-specific biases (*e.g.*, chest tubes, loculated pneumothorax for NIH; subtypes of calcifications for RSNA & VinDr Mammo), capturing a more granular characterization of biases. Unlike the keyword extraction or tagging models, which struggle with missing or insufficient attributes, LADDER leverages LLM-driven latent medical knowledge to generate comprehensive hypotheses. Such fine-grained detection of contextual biases, including subtypes, allows LADDER to for the detection of patterns that would be difficult to detect without domain expertise. Refer to Appendix A.12.3, A.12.2 and A.12.6 for detailed qualitative results, the hypotheses closest to the ground truth biases, and the influence of biased attributes via CLIP score, respectively.

**RQ3: Biased attributes discovery across**

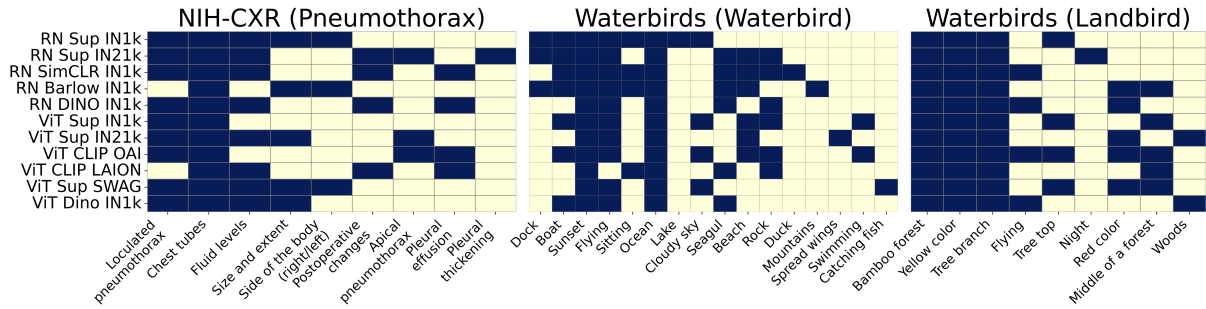


Figure 9: Biased attributes discovered by LADDER show consistent biases across architectures and pretraining. Several attributes (e.g., ocean, lake, beach etc.) represent the same visual concepts (water bodies) denoting the groundtruth bias. Bright and light colors indicate attribute presence and absence, respectively.

Table 1: Impact of captioners on LADDER’s performance for RN Sup IN1k classifier. Though GPT-4o is expensive, its quality is better than others.

Method	Waterbirds		CelebA	
	Mean Acc	WGA	Mean Acc	WGA
BLIP (Li et al., 2022)	93.1	91.4	89.8	88.9
BLIP2 (Li et al., 2023a)	93.3	91.6	89.8	89.2
ClipCap (Mokady et al., 2021)	93.7	91.8	88.3	87.4
GPT-4o (Wu et al., 2024)	<b>94.2</b>	<b>93.1</b>	<b>91.4</b>	<b>90.3</b>

**architectures/pre-training methods.** In this setup, we extract biases using LADDER on a range of model architectures (both ResNet50 and ViT), initializing  $f$  (the model to be probed) with diverse pretraining methods, including SimCLR (Chen et al., 2020), Barlow Twins (Zbontar et al., 2021), DINO (Caron et al., 2021), and CLIP (Radford et al., 2021). These methods are pretrained on datasets e.g., ImageNet-1K (IN1k) (Deng et al., 2009), ImageNet-21K (IN21k) (Ridnik et al., 2021), SWAG (Singh et al., 2022), LAION-2B (Schuhmann et al., 2022), and OpenAI-CLIP (OAI) (Radford et al., 2021). Yang et al. (2023) shows that every ERM-trained classifier ( $f$ ) exhibits low WGA irrespective of architecture/pre-training due to consistently learning similar biases. Figure 9 shows that LADDER, leveraging LLM-driven reasoning and *domain knowledge*, consistently identifies similar biases across different architectures, pretraining methods, and datasets. In the NIH dataset, LADDER identifies mostly key attributes such as chest tubes, fluid levels etc. Also, in the Waterbirds dataset, LADDER detects attributes e.g., ocean and bamboo forest consistently, showing the correlation of the spurious backgrounds with class labels and the ground truth biases. Appendix A.12.8 lists more results.

**RQ4: Mitigating biases using LADDER.** Tab. 2 shows that LADDER outperforms other bias mitiga-

tion baselines in estimating WGA, without requiring the expensive ground truth shortcut attributes, for both training and validation datasets across CNN models (EN-B5 for Mammograms and RN Sup IN1k for the rest). LADDER achieves a WGA of 91.4%, 76.4% and 82.5% – a 3.6%, 7.3% and 21.1% improvement ( $\uparrow$ ) over DFR in the Waterbirds, RSNA, and VinDr datasets, respectively. For NIH, LADDER outperforms JTT and DFR by 8.2% and 7.4%, respectively. Appendix A.12.4 illustrates further analysis with an additional 9 baselines. Fig. 15 shows LADDER’s consistent performance gain across various architectures and pre-training methods. Tab. 11 in Appendix A.12.7 shows that LADDER outperforms Li et al. (2023b) on multi-shortcut benchmark UrbanCars. Leveraging LLMs’ advanced reasoning, LADDER accurately derives pseudo labels for the biased attributes from hypotheses to identify true model biases. LADDER then applies targeted bias mitigation by fine-tuning the last layer, resulting in a systematic debiased model per hypothesis. This efficient strategy effectively enhances model performance across the biases, modalities, and architectures.

Table 2: Error mitigation results (WGA) for EN-B5 for mammograms and RN Sup IN1k for the rest. We bold-face and underline the best and second-best results. We compare with 9 additional baselines in A.12.4.

Method	Waterbirds	CelebA	NIH	RSNA	VinDr
ERM	69.1 $\pm$ 1.2	62.2 $\pm$ 1.5	60.3 $\pm$ 0.0	69.8 $\pm$ 0.0	45.6 $\pm$ 0.0
JTT	84.5 $\pm$ 0.3	87.2 $\pm$ 7.5	70.4 $\pm$ 0.0	68.5 $\pm$ 0.0	66.1 $\pm$ 0.0
GroupDRO	87.1 $\pm$ 1.3	<u>88.1<math>\pm</math>0.7</u>	71.1 $\pm$ 0.0	<u>72.3<math>\pm</math>0.0</u>	67.1 $\pm$ 0.0
CVaRDRO	85.4 $\pm$ 2.3	83.1 $\pm$ 1.5	<u>71.3<math>\pm</math>0.0</u>	71.7 $\pm$ 0.0	67.1 $\pm$ 0.0
LIF	75.2 $\pm$ 0.7	63.0 $\pm$ 4.4	61.6 $\pm$ 0.0	66.4 $\pm$ 0.0	64.5 $\pm$ 0.0
DFR	<u>88.2<math>\pm</math>0.3</u>	87.1 $\pm$ 1.1	70.5 $\pm$ 0.0	71.2 $\pm$ 0.0	<u>68.1<math>\pm</math>0.0</u>
<b>LADDER</b>	<b>91.4<math>\pm</math>0.8</b>	<b>88.9<math>\pm</math>0.4</b>	<b>76.2<math>\pm</math>0.0</b>	<b>76.4<math>\pm</math>0.0</b>	<b>82.5<math>\pm</math>0.0</b>

**RQ5: Relaxing the dependency on captions.** To reduce LADDER’s reliance on captions/reports, we leverage instruction-tuned models to generate tex-

492 tual descriptions for the correctly classified samples. Specifically, we use LLaVA-1.5 7B (Liu  
 493 et al., 2024) for natural images and RaDialog (Pel-  
 494 legrini et al., 2023) and cheXagent (Chen et al.,  
 495 2024b) for CXRs to probe RN Sup IN1k classifier.  
 496 Refer to Appendix A.8 for the utilized prompts.  
 497 LADDER’s LLM pipeline utilizes these generated  
 498 descriptions to identify biased attributes. Recall  
 499 we aim to detect biases consistently present in  
 500 correctly classified instances. Figure 5 compares  
 501 the biases identified using LADDER’s retrieval  
 502 pipeline (captions/reports) vs. those detected via  
 503 instruction-tuned models. Figure 6(a) compares  
 504 Precision@10 for LADDER under both settings,  
 505 while Figure 6(b) evaluates the WGA metric, evalu-  
 506 ating the bias discovery and mitigation quantita-  
 507 tively, respectively. For natural images, LADDER  
 508 with instruction-tuned models perform compara-  
 509 bly to the standard pipeline using captions. For  
 510 CXRs, the retrieval-based approach utilizing actual  
 511 reports outperforms methods using cheXagent and  
 512 RaDialog, highlighting the importance of domain-  
 513 specific reports in medical imaging. Thus, us-  
 514 ing models *e.g.*, LLaVA can eliminate LADDER’s  
 515 need for captions. However, this approach is chal-  
 516 lenging for 2D mammograms and dermatology  
 517 imaging (Alzubaidi et al., 2021) etc. where robust  
 518 instruction-tuned models are lacking. In such cases,  
 519 LADDER’s retrieval pipeline remains highly adapt-  
 520 able and shows broad applicability. Thus, a trade-  
 521 off emerges: models can either leverage explicit  
 522 radiology reports for bias identification or develop  
 523 robust VLRs to reduce dependence on reports.  
 524

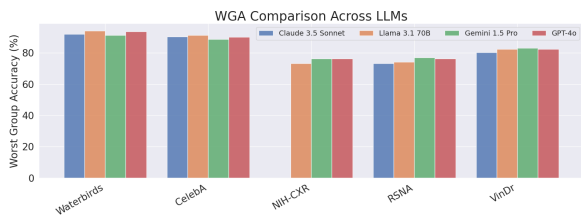


Figure 10: WGA comparison across different LLMs for bias mitigation by LADDER with RN Sup IN1k for natural images and CXRs, and EN-B5 for mammograms. GPT-4o and Gemini excel in medical imaging tasks.

525 **RQ6: Detecting biases beyond captions/reports.**  
 526 While prior work (Boyd et al., 2023) highlights bi-  
 527 ases in EHR and medical imaging headers (*e.g.*,  
 528 DICOMs), LADDER extends bias detection be-  
 529 yond captions. We use metadata from the RSNA-  
 530 Mammo dataset, which includes metadata *e.g.*,  
 531 BIRADS(0-2), age, implant, view (CC or MLO),

532 laterality (left or right breast), machine\_id, and  
 533 site\_id. Also, the DICOM headers provide at-  
 534 tributes *e.g.*, photometric interpretation, VOI LUT,  
 535 and pixel intensity relationships. We probe the  
 536 same EN-B5 classifier to find attributes consistently  
 537 present in correctly classified samples, whose ab-  
 538 sence results in a performance drop. By listing  
 539 each sample’s metadata to a Python dictionary (re-  
 540 fer to Appendix A.9) and using LADDER’s LLM  
 541 pipeline (Sec. 3.2), we generate hypotheses about  
 542 the biased attributes; we then validate their impact  
 543 on the classifier’s performance based on the pres-  
 544 ence/absence of these attributes, with their ground  
 545 truth values from the metadata. Figure 7 shows that  
 546 LADDER detects an age bias (a 19.5% accuracy gap  
 547 for patients aged 70+ vs. the rest) and a 10% gap to  
 548 different photometric interpretations (Monochrome  
 549 1 vs. Monochrome 2). This finding aligns with ex-  
 550 isting evidence of age bias in oncology (Tasci et al.,  
 551 2022). Existing methods lack LLM-based reason-  
 552 ing, limiting them to fixed attributes or clustering,  
 553 while LADDER uses LLMs to reason across meta-  
 554 data for comprehensive analysis.

## 6 Ablations and Additional Results

555 Table 1 compares LADDER’s performance across  
 556 different captioning methods, while Fig. 10 presents  
 557 the WGA of LADDER for various LLMs. Due to  
 558 space constraints, we provide detailed analyses in  
 559 Appendices A.12.10 and A.12.12. Additionally,  
 560 Appendices A.12.11, A.12.13 and A.12.14 include  
 561 ablation studies on slices discovered using different  
 562 LLMs, their computational costs, and the impact  
 563 of different VLRs on LADDER. Appendix A.12.9  
 564 demonstrates LADDER’s ability to identify biases  
 565 in the ImageNet dataset (multiclass classification),  
 566 while Appendix A.12.5 shows how these identified  
 567 attributes improve CLIP’s zero-shot accuracy.  
 568

## 7 Conclusion

569 We introduce LADDER, a novel LLM-driven  
 570 method for error slice discovery and bias mitiga-  
 571 tion for vision classifiers. Unlike prior methods  
 572 that rely on predefined attributes or unsupervised  
 573 clustering, LADDER leverages LLM’s reasoning to  
 574 detect coherent error slices without requiring ex-  
 575 plicit annotations from any off-the-shelf pretrained  
 576 classifier. Next, it mitigates multiple biases through  
 577 pseudo-label generation and attribute rebalancing.  
 578 Extensive evaluations on 6 datasets show LADDER  
 579 ’s effectiveness, outperforming existing baselines.  
 580



## 581 Limitations

582 While LADDER demonstrates superior performance  
583 in bias discovery and mitigation, we outline the  
584 limitations of our work and potential areas for im-  
585 provement: **1. Dependence on captions for bias**  
586 **discovery:** LADDER primarily relies on captions  
587 to identify biases, which may not be suitable for  
588 domains with sparse or limited textual descriptions.  
589 While we introduce a workaround using instruction-  
590 tuned models *e.g.*, LLaVA for specific applications,  
591 future research will explore reducing language de-  
592 pendence across broader domains. **2. Potential**  
593 **bias in pretrained models:** LADDER utilizes pre-  
594 trained models such as CLIP and LLMs, which  
595 inherently reflect biases present in their training  
596 data. This dependency may influence the bias dis-  
597 covery process and potentially undermine fairness  
598 objectives. Addressing and mitigating these inher-  
599 ent biases in foundational models is an important  
600 direction for future research. **3. Lack of human**  
601 **oversight in bias discovery:** To prevent the in-  
602 troduction of additional bias, LADDER automates  
603 the discovery phase without human intervention.  
604 Instead, domain experts (*e.g.*, clinicians) validate  
605 the identified biases prior to mitigation. While this  
606 strategy minimizes human-induced bias during dis-  
607 covery, it introduces subjectivity in the validation  
608 phase. Enhancing and standardizing this validation  
609 process remains a key focus for future work.

## 610 Ethical Considerations

611 We strongly adhere to ethical standards in the han-  
612 dling of medical data, the use of language models,  
613 and the implementation of machine learning meth-  
614 ods. We provide the following details: **1. Medical**  
615 **datasets:** All medical datasets used in this study, in-  
616 cluding MIMIC-CXR, RSNA-Mammo, and VinDr-  
617 Mammo, are anonymized and publicly available.  
618 We strictly follow the respective data-use agree-  
619 ments and ethical guidelines associated with each  
620 dataset. **2. Language models for medical tasks:**  
621 The large language models (LLMs) employed for  
622 medical applications adhere to the guidelines es-  
623 tablished for MIMIC<sup>1</sup>. Specifically, we use GPT-  
624 4o (Wu et al., 2024) via Azure OpenAI service as  
625 LLM for NIH in the main experiments. For abla-  
626 tions, we use Google’s Gemini via Vertex AI. For  
627 LLaMA, we set up the model on a local machine.  
628 No information from NIH datasets was processed

<sup>1</sup><https://physionet.org/news/post/gpt-responsible-use>

629 using language models not covered by these guide-  
630 lines, such as Claude. **3. Classifier models and**  
631 **codebase:** All classifiers used in this research are  
632 standard architectures and publicly available mod-  
633 els, ensuring reproducibility and transparency. We  
634 list them in detail in Appendix A.10. **4. Vision-**  
635 **Language representations (VLRs):** All VLRs  
636 utilized in this study are publicly available, and we  
637 list the corresponding resources in Appendix A.10.  
638 We adhere strictly to the license terms specified by  
639 the creators of these resources.

## 640 Broader Impact

641 The development and deployment of LADDER have  
642 potential implications for AI applications in medi-  
643 cal and general computer vision tasks. We outline  
644 the broader impacts as follows: **1. Medical ap-**  
645 **lications and patient outcomes:** LADDER can  
646 improve the robustness and interpretability of vi-  
647 sion models in medical imaging. By identifying  
648 and mitigating biases, it can lead to more reliable  
649 diagnostic tools, ultimately enhancing patient care  
650 and reducing diagnostic disparities. **2. Bias detec-**  
651 **tion and fairness:** LADDER offers a generalizable  
652 approach to uncovering and addressing systematic  
653 biases across datasets. This can contribute to the  
654 development of fairer AI models, particularly in  
655 domains prone to dataset biases, such as healthcare  
656 and social applications. **3. Continuous auditing**  
657 **and bias mitigation:** LADDER can act as an au-  
658 ditor for any pretrained network in a continuous  
659 manner. By running it on a dataset, it can identify  
660 and mitigate biases using language. Whenever a  
661 bias can be traced in language, LADDER can de-  
662 tect it with its superior reasoning capabilities and  
663 domain knowledge.

## 664 References

- 665 Laith Alzubaidi, Muthana Al-Amidie, Ahmed Al-  
666 Asadi, Amjad J Humaidi, Omran Al-Shamma, Mo-  
667 hammed A Fadhel, Jinglan Zhang, Jesus Santamaría,  
668 and Ye Duan. 2021. Novel transfer learning approach  
669 for medical imaging with limited labeled data. *Cancer*, 13(7):1590. 670
- 671 Martin Arjovsky, Léon Bottou, Ishaan Gulrajani, and  
672 David Lopez-Paz. 2020. *Invariant risk minimization*.  
673 *Preprint*, arXiv:1907.02893.
- 674 Andrew D Boyd, Rosa Gonzalez-Guarda, Katharine  
675 Lawrence, Crystal L Patil, Miriam O Ezenwa,  
676 Emily C O’Brien, Hyung Paek, Jordan M  
677 Braciszewski, Oluwaseun Adeyemi, Allison M

678	Cuthel, et al. 2023. Potential bias and lack of generalizability in electronic health record data: reflections on health equity from the national institutes of health pragmatic trials collaboratory. <i>Journal of the American Medical Informatics Association</i> , 30(9):1561–1566.	Alexey Dosovitskiy, Lucas Beyer, Alexander Kolesnikov, Dirk Weissenborn, Xiaohua Zhai, Thomas Unterthiner, Mostafa Dehghani, Matthias Minderer, Georg Heigold, Sylvain Gelly, et al. 2020. An image is worth 16x16 words: Transformers for image recognition at scale. <i>arXiv preprint arXiv:2010.11929</i> .	735
679			736
680			737
681			738
682			739
683			740
684	Kaidi Cao, Colin Wei, Adrien Gaidon, Nikos Arechiga, and Tengyu Ma. 2019. Learning imbalanced datasets with label-distribution-aware margin loss. <i>Advances in neural information processing systems</i> , 32.	Abhimanyu Dubey, Abhinav Jauhri, Abhinav Pandey, Abhishek Kadian, Ahmad Al-Dahle, Aiesha Letman, Akhil Mathur, Alan Schelten, Amy Yang, Angela Fan, et al. 2024. The llama 3 herd of models. <i>arXiv preprint arXiv:2407.21783</i> .	742
685			743
686			744
687			745
688	Mathilde Caron, Hugo Touvron, Ishan Misra, Hervé Jégou, Julien Mairal, Piotr Bojanowski, and Armand Joulin. 2021. Emerging properties in self-supervised vision transformers. In <i>Proceedings of the IEEE/CVF international conference on computer vision</i> , pages 9650–9660.	John Duchi and Hongseok Namkoong. 2021. <a href="#">Learning models with uniform performance via distributionally robust optimization</a> . <i>The Annals of Statistics</i> , 49.	746
689			747
690			748
691			749
692			
693			
694	Muxi Chen, Yu Li, and Qiang Xu. 2024a. Hibug: on human-interpretable model debug. <i>Advances in Neural Information Processing Systems</i> , 36.	Sabri Eyuboglu, Maya Varma, Khaled Saab, Jean-Benoit Delbrouck, Christopher Lee-Messer, Jared Dunnmon, James Zou, and Christopher Ré. 2022. Domino: Discovering systematic errors with cross-modal embeddings. <i>arXiv preprint arXiv:2203.14960</i> .	750
695			751
696			752
697	Ting Chen, Simon Kornblith, Mohammad Norouzi, and Geoffrey Hinton. 2020. A simple framework for contrastive learning of visual representations. In <i>International conference on machine learning</i> , pages 1597–1607. PMLR.	Shantanu Ghosh, Clare B. Poynton, Shyam Visweswaran, and Kayhan Batmanghelich. 2024. Mammo-clip: A vision language foundation model to enhance data efficiency and robustness in mammography. In <i>Medical Image Computing and Computer Assisted Intervention – MICCAI 2024</i> , pages 632–642, Cham. Springer Nature Switzerland.	753
698			754
699			755
700			
701			
702	Zhihong Chen, Maya Varma, Jean-Benoit Delbrouck, Magdalini Paschali, Louis Blankemeier, Dave Van Veen, Jeya Maria Jose Valanarasu, Alaa Youssef, Joseph Paul Cohen, Eduardo Pontes Reis, et al. 2024b. Chexagent: Towards a foundation model for chest x-ray interpretation. <i>arXiv preprint arXiv:2401.12208</i> .	Chuan Guo, Tom Goldstein, Awni Hannun, and Laurens Van Der Maaten. 2019. Certified data removal from machine learning models. <i>arXiv preprint arXiv:1911.03030</i> .	756
703			757
704			758
705			759
706			760
707			761
708			762
709	Yin Cui, Menglin Jia, Tsung-Yi Lin, Yang Song, and Serge Belongie. 2019. Class-balanced loss based on effective number of samples. In <i>Proceedings of the IEEE/CVF conference on computer vision and pattern recognition</i> , pages 9268–9277.	Chuan Guo, Tom Goldstein, Awni Hannun, and Laurens Van Der Maaten. 2020. Certified data removal from machine learning models. In <i>Proceedings of the 37th International Conference on Machine Learning, ICML’20</i> . JMLR.org.	763
710			764
711			765
712			766
713			
714	Jia Deng, Wei Dong, Richard Socher, Li-Jia Li, Kai Li, and Li Fei-Fei. 2009. Imagenet: A large-scale hierarchical image database. In <i>2009 IEEE conference on computer vision and pattern recognition</i> , pages 248–255. Ieee.	Kaiming He, Xiangyu Zhang, Shaoqing Ren, and Jian Sun. 2016. Deep residual learning for image recognition. In <i>Proceedings of the IEEE conference on computer vision and pattern recognition</i> , pages 770–778.	767
715			768
716			769
717			770
718			771
719	Greg d’Eon, Jason d’Eon, James R Wright, and Kevin Leyton-Brown. 2022. The spotlight: A general method for discovering systematic errors in deep learning models. In <i>Proceedings of the 2022 ACM Conference on Fairness, Accountability, and Transparency</i> , pages 1962–1981.	Shih-Cheng Huang, Liyue Shen, Matthew P Lungren, and Serena Yeung. 2021. Gloria: A multimodal global-local representation learning framework for label-efficient medical image recognition. In <i>Proceedings of the IEEE/CVF International Conference on Computer Vision</i> , pages 3942–3951.	772
720			773
721			774
722			775
723			776
724			
725	Moreno D’Incà, Elia Peruzzo, Massimiliano Mancini, Dejia Xu, Vidit Goel, Xingqian Xu, Zhangyang Wang, Humphrey Shi, and Nicu Sebe. 2024. Openbias: Open-set bias detection in text-to-image generative models. In <i>Proceedings of the IEEE/CVF Conference on Computer Vision and Pattern Recognition</i> , pages 12225–12235.	Alistair EW Johnson, Tom J Pollard, Seth J Berkowitz, Nathaniel R Greenbaum, Matthew P Lungren, Chihying Deng, Roger G Mark, and Steven Horng. 2019. MIMIC-CXR, a de-identified publicly available database of chest radiographs with free-text reports. <i>Scientific data</i> , 6(1):317.	777
726			778
727			779
728			780
729			781
730			782
731			
732	Frédéric Docquier and Hillel Rapoport. 2012. Globalization, brain drain, and development. <i>Journal of economic literature</i> , 50(3):681–730.		783
733			784
734			785

789	Bingyi Kang, Saining Xie, Marcus Rohrbach, Zhicheng Yan, Albert Gordo, Jiashi Feng, and Yannis Kalantidis. 2020. <a href="#">Decoupling representation and classifier for long-tailed recognition</a> . In <i>International Conference on Learning Representations</i> .	846
790		847
791		848
792		849
793		850
794	Michael P Kim, Amirata Ghorbani, and James Zou. 2019. Multiaccuracy: Black-box post-processing for fairness in classification. In <i>Proceedings of the 2019 AAAI/ACM Conference on AI, Ethics, and Society</i> , pages 247–254.	851
795		
796		852
797		853
798		854
799	Younghyun Kim, Sangwoo Mo, Minkyu Kim, Kyungmin Lee, Jaeho Lee, and Jinwoo Shin. 2024. Discovering and mitigating visual biases through keyword explanation. In <i>Proceedings of the IEEE/CVF Conference on Computer Vision and Pattern Recognition</i> , pages 11082–11092.	855
800		856
801		857
802		858
803		
804		859
805	Polina Kirichenko, Pavel Izmailov, and Andrew Gordon Wilson. 2022. Last layer re-training is sufficient for robustness to spurious correlations. <i>arXiv preprint arXiv:2204.02937</i> .	860
806		861
807		
808		862
809	Ranjay Krishna, Yuke Zhu, Oliver Groth, Justin Johnson, Kenji Hata, Joshua Kravitz, Stephanie Chen, Yannis Kalantidis, Li-Jia Li, David A. Shamma, Michael S. Bernstein, and Li Fei-Fei. 2017. <a href="#">Visual genome: Connecting language and vision using crowdsourced dense image annotations</a> . <i>Int. J. Comput. Vision</i> , 123(1):32–73.	863
810		864
811		865
812		
813		866
814		867
815		868
816	Haoliang Li, Sinno Jialin Pan, Shiqi Wang, and Alex C. Kot. 2018. Domain generalization with adversarial feature learning. In <i>Proceedings of the IEEE Conference on Computer Vision and Pattern Recognition (CVPR)</i> .	869
817		870
818		871
819		872
820		
821	Junnan Li, Dongxu Li, Silvio Savarese, and Steven Hoi. 2023a. Blip-2: Bootstrapping language-image pre-training with frozen image encoders and large language models. In <i>International conference on machine learning</i> , pages 19730–19742. PMLR.	873
822		874
823		875
824		876
825		877
826	Junnan Li, Dongxu Li, Caiming Xiong, and Steven Hoi. 2022. Blip: Bootstrapping language-image pre-training for unified vision-language understanding and generation. In <i>International conference on machine learning</i> , pages 12888–12900. PMLR.	878
827		879
828		880
829		881
830		882
831	Zhiheng Li, Ivan Evtimov, Albert Gordo, Caner Hazirbas, Tal Hassner, Cristian Canton Ferrer, Chenliang Xu, and Mark Ibrahim. 2023b. A whac-a-mole dilemma: Shortcuts come in multiples where mitigating one amplifies others. In <i>Proceedings of the IEEE/CVF Conference on Computer Vision and Pattern Recognition</i> , pages 20071–20082.	883
832		884
833		885
834		886
835		
836		887
837		888
838	Weixin Liang and James Zou. 2022. Metashift: A dataset of datasets for evaluating contextual distribution shifts and training conflicts. <i>arXiv preprint arXiv:2202.06523</i> .	889
839		890
840		891
841		
842	Tsung-Yi Lin, Priya Goyal, Ross Girshick, Kaiming He, and Piotr Dollar. 2017. Focal loss for dense object detection. In <i>Proceedings of the IEEE International Conference on Computer Vision (ICCV)</i> .	892
843		893
844		894
845		895
		896
		897
	Evan Z Liu, Behzad Haghgoo, Annie S Chen, Aditi Raghunathan, Pang Wei Koh, Shiori Sagawa, Percy Liang, and Chelsea Finn. 2021. Just train twice: Improving group robustness without training group information. In <i>International Conference on Machine Learning</i> , pages 6781–6792. PMLR.	
	Haotian Liu, Chunyuan Li, Qingyang Wu, and Yong Jae Lee. 2024. Visual instruction tuning. <i>Advances in neural information processing systems</i> , 36.	
	Ziwei Liu, Ping Luo, Xiaogang Wang, and Xiaoou Tang. 2015. Deep learning face attributes in the wild. <i>Proceedings of the IEEE International Conference on Computer Vision (ICCV)</i> .	
	Ziwei Liu, Ping Luo, Xiaogang Wang, and Xiaoou Tang. 2018. Large-scale celebfaces attributes (celeba) dataset. <i>Retrieved August, 15(2018):11</i> .	
	Mazda Moayeri, Keivan Rezaei, Maziar Sanjabi, and Soheil Feizi. 2023. Text-to-concept (and back) via cross-model alignment. In <i>International Conference on Machine Learning</i> , pages 25037–25060. PMLR.	
	Ron Mokady, Amir Hertz, and Amit H Bermano. 2021. Clipcap: Clip prefix for image captioning. <i>arXiv preprint arXiv:2111.09734</i> .	
	Nihal Murali, Aahlad Puli, Ke Yu, Rajesh Ranganath, and Kayhan Batmanghelich. 2023. Beyond distribution shift: Spurious features through the lens of training dynamics. <i>arXiv preprint arXiv:2302.09344</i> .	
	Junhyun Nam, Hyuntak Cha, Sungsoo Ahn, Jaeho Lee, and Jinwoo Shin. 2020. Learning from failure: Debiasing classifier from biased classifier. <i>Advances in Neural Information Processing Systems</i> , 33:20673–20684.	
	Hieu T Nguyen, Ha Q Nguyen, Hieu H Pham, Khanh Lam, Linh T Le, Minh Dao, and Van Vu. 2023. Vindr-mammo: A large-scale benchmark dataset for computer-aided diagnosis in full-field digital mammography. <i>Scientific Data</i> , 10(1):277.	
	Priya K Palanisamy, Bhawna Dev, and MC Sheela. 2023. Reporting template: Mammogram, usg, mri. In <i>Holistic Approach to Breast Disease</i> , pages 71–75. Springer.	
	Chantal Pellegrini, Ege Özsoy, Benjamin Busam, Nassir Navab, and Matthias Keicher. 2023. Radialog: A large vision-language model for radiology report generation and conversational assistance. <i>arXiv preprint arXiv:2311.18681</i> .	
	Alec Radford, Jong Wook Kim, Chris Hallacy, Aditya Ramesh, Gabriel Goh, Sandhini Agarwal, Girish Sastry, Amanda Askell, Pamela Mishkin, Jack Clark, et al. 2021. Learning transferable visual models from natural language supervision. In <i>International conference on machine learning</i> , pages 8748–8763. PMLR.	

898	Keivan Rezaei, Mehrdad Saberi, Mazda Moayeri, and Soheil Feizi. 2023. Prime: Prioritizing interpretability in failure mode extraction. <i>arXiv preprint arXiv:2310.00164</i> .	953
899		954
900		955
901		956
902	Tal Ridnik, Emanuel Ben-Baruch, Asaf Noy, and Lihi Zelnik-Manor. 2021. Imagenet-21k pretraining for the masses. <i>arXiv preprint arXiv:2104.10972</i> .	957
903		958
904		959
905	Shiori Sagawa, Pang Wei Koh*, Tatsunori B. Hashimoto, and Percy Liang. 2020. <b>Distributionally robust neural networks</b> . In <i>International Conference on Learning Representations</i> .	960
906		961
907		962
908		963
909	Christoph Schuhmann, Romain Beaumont, Richard Vencu, Cade Gordon, Ross Wightman, Mehdi Cherti, Theo Coombes, Aarush Katta, Clayton Mullis, Mitchell Wortsman, et al. 2022. Laion-5b: An open large-scale dataset for training next generation image-text models. <i>Advances in Neural Information Processing Systems</i> , 35:25278–25294.	964
910		965
911		966
912		967
913		968
914		969
915		970
916	Mannat Singh, Laura Gustafson, Aaron Adcock, Vinicius de Freitas Reis, Bugra Gedik, Raj Prateek Kosaraju, Dhruv Mahajan, Ross Girshick, Piotr Dollár, and Laurens Van Der Maaten. 2022. Revisiting weakly supervised pre-training of visual perception models. In <i>Proceedings of the IEEE/CVF Conference on Computer Vision and Pattern Recognition</i> , pages 804–814.	971
917		972
918		973
919		974
920		975
921		976
922		977
923		978
924	Sahil Singla, Besmira Nushi, Shital Shah, Ece Kamar, and Eric Horvitz. 2021. Understanding failures of deep networks via robust feature extraction. In <i>Proceedings of the IEEE/CVF Conference on Computer Vision and Pattern Recognition</i> , pages 12853–12862.	979
925		980
926		981
927		982
928		983
929	Nimit Sohoni, Jared Dunnmon, Geoffrey Angus, Albert Gu, and Christopher Ré. 2020. No subclass left behind: Fine-grained robustness in coarse-grained classification problems. <i>Advances in Neural Information Processing Systems</i> , 33:19339–19352.	984
930		985
931		986
932		987
933		988
934	Mingxing Tan and Quoc Le. 2019. Efficientnet: Rethinking model scaling for convolutional neural networks. In <i>International conference on machine learning</i> , pages 6105–6114. PMLR.	989
935		990
936		991
937		992
938	Erdal Tasci, Ying Zhuge, Kevin Camphausen, and Andra V Krauze. 2022. Bias and class imbalance in oncologic data—towards inclusive and transferrable ai in large scale oncology data sets. <i>Cancers</i> , 14(12):2897.	993
939		994
940		995
941		996
942		997
943	Gemini Team, M Reid, N Savinov, D Teplyashin, Lepikhin Dmitry, T Lillicrap, JB Alayrac, R Soricut, A Lazaridou, O Firat, et al. 2024. Gemini 1.5: Unlocking multimodal understanding across millions of tokens of context. in arxiv [cs. cl]. arxiv.	998
944		999
945		1000
946		1001
947		1002
948	Vladimir Vapnik. 1999. <i>The Nature of Statistical Learning Theory</i> . Springer.	1003
949		1004
950	Catherine Wah, Steve Branson, Peter Welinder, Pietro Perona, and Serge Belongie. 2011. The caltech-ucsd birds-200-2011 dataset.	1005
951		1006
952		1007
	Xiaosong Wang, Yifan Peng, Le Lu, Zhiyong Lu, Mohammadhadi Bagheri, and Ronald M Summers. 2017. Chestx-ray8: Hospital-scale chest x-ray database and benchmarks on weakly-supervised classification and localization of common thorax diseases. In <i>Proceedings of the IEEE conference on computer vision and pattern recognition</i> , pages 2097–2106.	
	Zifeng Wang, Zhenbang Wu, Dinesh Agarwal, and Jimeng Sun. 2022. Medclip: Contrastive learning from unpaired medical images and text. <i>arXiv preprint arXiv:2210.10163</i> .	
	Xuesong Wen, Jianjun Li, and Liyuan Yang. 2024. Breast cancer diagnosis method based on cross-mammogram four-view interactive learning. <i>Tomography</i> , 10(6):848–868.	
	Chaoyi Wu, Xiaoman Zhang, Ya Zhang, Yanfeng Wang, and Weidi Xie. 2023. Medklip: Medical knowledge enhanced language-image pre-training for x-ray diagnosis. In <i>Proceedings of the IEEE/CVF International Conference on Computer Vision</i> , pages 21372–21383.	
	Yiqi Wu, Xiaodan Hu, Ziming Fu, Siling Zhou, and Jiangong Li. 2024. Gpt-4o: Visual perception performance of multimodal large language models in piglet activity understanding. <i>arXiv preprint arXiv:2406.09781</i> .	
	Yuzhe Yang, Haoran Zhang, Dina Katabi, and Marzyeh Ghassemi. 2023. Change is hard: A closer look at subpopulation shift. <i>arXiv preprint arXiv:2302.12254</i> .	
	Huaxiu Yao, Yu Wang, Sai Li, Linjun Zhang, Weixin Liang, James Zou, and Chelsea Finn. 2022. Improving out-of-distribution robustness via selective augmentation. In <i>International Conference on Machine Learning</i> , pages 25407–25437. PMLR.	
	Sriram Yenamandra, Pratik Ramesh, Viraj Prabhu, and Judy Hoffman. 2023. Facts: First amplify correlations and then slice to discover bias. In <i>IEEE/CVF International Conference in Computer Vision (ICCV)</i> .	
	Kihyun You, Jawook Gu, Jiyeon Ham, Beomhee Park, Jiho Kim, Eun K Hong, Woonhyuk Baek, and Byungseok Roh. 2023. Cxr-clip: Toward large scale chest x-ray language-image pre-training. In <i>International Conference on Medical Image Computing and Computer-Assisted Intervention</i> , pages 101–111. Springer.	
	Jure Zbontar, Li Jing, Ishan Misra, Yann LeCun, and Stéphane Deny. 2021. Barlow twins: Self-supervised learning via redundancy reduction. In <i>International conference on machine learning</i> , pages 12310–12320. PMLR.	
	Hongyi Zhang, Moustapha Cisse, Yann N. Dauphin, and David Lopez-Paz. 2018. <b>mixup: Beyond empirical risk minimization</b> . In <i>International Conference on Learning Representations</i> .	

1008	Yuhui Zhang, Jeff Z HaoChen, Shih-Cheng Huang,	<b>NIH chestXrays</b>	1055
1009	Kuan-Chieh Wang, James Zou, and Serena Yeung.	The <b>NIH ChestX-ray</b> dataset (Wang et al., 2017),	1056
1010	2023. <a href="#">Diagnosing and rectifying vision models using</a>	also known as ChestX-ray14, is a large dataset	1057
1011	<a href="#">language</a> . In <i>International Conference on Learning</i>	of chest radiographs (X-rays) provided by the Na-	1058
1012	<i>Representations (ICLR)</i> .	tional Institutes of Health (NIH). The dataset com-	1059
1013	Bolei Zhou, Agata Lapedriza, Aditya Khosla, Aude	prises 112,120 frontal-view X-ray images of 30,805	1060
1014	Oliva, and Antonio Torralba. 2017. <i>Places: A 10</i>	unique patients. Each image is associated with one	1061
1015	<i>million image database for scene recognition. IEEE</i>	or more of the 14 labeled thoracic diseases, which	1062
1016	<i>Transactions on Pattern Analysis and Machine Intel-</i>	include atelectasis, cardiomegaly, effusion, infil-	1063
1017	<i>ligence</i> .	tration, mass, nodule, pneumonia, pneumothorax,	1064
1018	<b>A Appendix</b>	consolidation, edema, emphysema, fibrosis, pleural	1065
1019	<b>A.1 Extended details on datasets</b>	thickening, and hernia. Previous works (Docquier	1066
1020	<b>Waterbirds</b>	and Rapoport, 2012) show that most pneumothorax	1067
1021	The <b>Waterbirds</b> dataset (Wah et al., 2011) is fre-	patients have a spurious correlation with the chest	1068
1022	quently employed in studies addressing spurious	drains. Chest drains are used to treat positive Pneu-	1069
1023	correlations. This binary classification dataset over-	mothorax cases. We adopt the strategy discussed	1070
1024	laps images from the Caltech-UCSD Birds-200-	in Murali et al. (2023) to annotate chest drains	1071
1025	2011 (CUB) dataset with backgrounds sourced	for each sample. We use the official train/val/test	1072
1026	from the Places dataset (Zhou et al., 2017). The	split (Wang et al., 2017).	1073
1027	primary task involves determining whether a bird	<b>RSNA breast mammograms</b>	1074
1028	depicted in an image is a landbird or a waterbird,	The <b>RSNA-Mammo</b> dataset <sup>2</sup> is a publicly avail-	1075
1029	with the background (water or land) as the spurious	able dataset containing 2D mammograms from	1076
1030	attribute. For consistency and comparability, we	11,913 patients, with 486 diagnosed cancer cases.	1077
1031	adhere to the train/validation/test splits utilized in	The task is to classify malignant cases from screen-	1078
1032	prior research (Guo et al., 2020).	ing mammograms. We use a 70/20/10 train/valida-	1079
1033	<b>CelebA</b>	tion/test split for evaluation as Ghosh et al. (2024).	1080
1034	The <b>CelebA</b> dataset (Liu et al., 2015) comprises	<b>VinDr breast mammograms</b>	1081
1035	over 200,000 images of celebrity faces. In the con-	The <b>VinDr-Mammo</b> dataset <sup>3</sup> (Nguyen et al., 2023)	1082
1036	text of spurious correlations research, this dataset	is a publicly available 2D mammogram dataset	1083
1037	is typically used for the binary classification task	of 5,000 exams (20,000 images) from Vietnam,	1084
1038	of predicting hair color (blond vs. non-blond), with	each with four views. It includes breast-level BI-	1085
1039	gender serving as the spurious correlation. In align-	RADS assessment categories (1-5), breast density	1086
1040	ment with previous studies (Guo et al., 2020), we	categories (A-D), and annotations for mammo-	1087
1041	use the standard dataset splits. The CelebA dataset	graphic attributes (e.g., mass, calcifications). Fol-	1088
1042	is available under the Creative Commons Attribu-	lowing Wen et al. (2024), we classify patients with	1089
1043	tion 4.0 International license.	BI-RADS scores between 1 and 3 as normal and	1090
1044	<b>MetaShift</b>	those with scores of 4 and 5 as abnormal. We adopt	1091
1045	The <b>MetaShift</b> dataset (Liang and Zou, 2022)	the train-test split from Nguyen et al. (2023).	1092
1046	offers a flexible platform for generating image	<b>A.2 Extended details on slice discovery</b>	1093
1047	datasets based on the Visual Genome project (Kr-	<b>algorithms</b>	1094
1048	ishna et al., 2017). Our experiments utilize the	<b>Domino.</b> Domino (Eyuboglu et al., 2022) identi-	1095
1049	pre-processed <i>Cat vs. Dog</i> dataset, designed to	fies systematic errors in machine learning models	1096
1050	differentiate between cats and dogs. The dataset	by leveraging cross-modal embeddings. It oper-	1097
1051	features the image background as a spurious at-	ates in three main steps: embedding, slicing, and	1098
1052	tribute, with cats typically appearing indoors and	describing.	1099
1053	dogs outdoors. We use the "unmixed" version of		
1054	this dataset, as provided by the authors' codebase.		

<sup>2</sup><https://www.kaggle.com/competitions/rsna-breast-cancer-detection>  
<sup>3</sup><https://www.physionet.org/content/vindr-mammo/1.0.0/>

1100	1. <b>Embedding:</b> Domino uses cross-modal models ( <i>e.g.</i> , CLIP) to embed inputs and text in the same latent space. This enables the incorporation of semantic meaning from text into input embeddings, which is crucial for identifying coherent slices.	1146
1101		1147
1102		1148
1103		1149
1104		1150
1105		
1106	2. <b>Slicing:</b> It employs an error-aware mixture model to detect underperforming regions within the embedding space. This model clusters the data based on embeddings, class labels, and model predictions to pinpoint areas where the model performance is subpar. The mixture model ensures that identified slices are coherent and relevant to model errors.	1151
1107		1152
1108		1153
1109		1154
1110		
1111		
1112		
1113		
1114	3. <b>Describing:</b> Domino generates natural language descriptions for the discovered slices. It creates prototype embeddings for each slice and matches them with text embeddings to describe the common characteristics of the slice. This step provides interpretable insights into why the model fails on these slices.	1155
1115		1156
1116		1157
1117		1158
1118		1159
1119		1160
1120		1161
1121		1162
1122	Domino’s approach improves slice coherence and generates meaningful slice descriptions.	1163
1123	<b>Facts.</b> Facts (Yenamandra et al., 2023) (First Amplify Correlations and Then Slice) aims to identify bias-conflicting slices in datasets through a two-stage process:	1164
1124		1165
1125		1166
1126		1167
1127	1. <b>Amplify Correlations:</b> This stage involves training a model with a high regularization term to amplify its reliance on spurious correlations present in the dataset. This step helps segregate biased-aligned from bias-conflicting samples by making the model fit a simpler, biased-aligned hypothesis.	1168
1128		1169
1129		1170
1130		1171
1131		1172
1132		1173
1133		1174
1134	2. <b>Correlation-aware Slicing:</b> In this stage, FACTS uses clustering techniques on the bias-amplified feature space to discover bias-conflicting slices. The method identifies subgroups where the spurious correlations do not hold, highlighting areas where the model underperforms due to these biases.	1175
1135		1176
1136		1177
1137		
1138		
1139		
1140		
1141	Facts leverages a combination of bias amplification and clustering to reveal underperforming data slices, providing a foundation for understanding and mitigating systematic biases in machine learning models.	1178
1142		1179
1143		1180
1144		1181
1145		1182
	<b>A.3 Extended details on error mitigation baselines</b>	1183
	We categorize the various bias mitigation algorithms and provide detailed descriptions for each category below.	1184
		1185
	<b>Vanilla</b>	1186
	The empirical risk minimization (ERM) algorithm, introduced by Vapnik (Vapnik, 1999), seeks to minimize the cumulative error across all samples.	1187
		1188
	<b>Subgroup Robust Methods</b>	1189
	<b>GroupDRO:</b> GroupDRO (Sagawa et al., 2020) propose Group Distributionally Robust Optimization (GroupDRO), which enhances ERM by prioritizing groups with higher error rates. <b>CVaRDRO:</b> Duchi and Namkoong (Duchi and Namkoong, 2021) introduce a variant of GroupDRO that dynamically assigns weights to data samples with the highest losses. <b>LfF:</b> LfF (Nam et al., 2020) concurrently trains two models: the first model is biased, and the second is de-biased by re-weighting the loss gradient. <b>Just Train Twice (JTT):</b> JTT (Liu et al., 2021) propose an approach that initially trains an ERM model to identify minority groups in the training set, followed by a second ERM model where the identified samples are re-weighted. <b>LISA:</b> LISA (Yao et al., 2022) utilizes invariant predictors through data interpolation within and across attributes. <b>Deep Feature Re-weighting (DFR):</b> DFR (Kirichenko et al., 2022) suggests first training an ERM model and then retraining the final layer using a balanced validation set with group annotations.	1190
		1191
		1192
		1193
		1194
		1195
		1196
		1197
		1198
		1199
		1200
		1201
		1202
		1203
		1204
		1205
		1206
		1207
		1208
		1209
		1210
		1211
		1212
		1213
		1214
		1215
		1216
		1217
		1218
		1219
		1220
		1221
		1222
		1223
		1224
		1225
		1226
		1227
		1228
		1229
		1230
		1231
		1232
		1233
		1234
		1235
		1236
		1237
		1238
		1239
		1240
		1241
		1242
		1243
		1244
		1245
		1246
		1247
		1248
		1249
		1250

## Imbalanced Learning

**Focal Loss (Focal):** Focal (Lin et al., 2017) introduces Focal Loss, which reduces the loss for well-classified samples and emphasizes difficult samples.

**Class-Balanced Loss (CBLoss):** CBLoss (Cui et al., 2019) suggests re-weighting by the inverse effective number of samples. **LDAM Loss (LDAM):** LDAM (Cao et al., 2019) employs a modified margin loss that preferentially weights minority samples. **Classifier Re-training (CRT):** CRT (Kang et al., 2020) decomposes representation learning and classifier training into two distinct stages, re-weighting the classifier using class-balanced sampling during the second stage. **ReWeightCRT:** ReWeightCRT (Kang et al., 2020) proposes a re-weighted variant of CRT.

### A.4 Learning Projection from classifier to VLR space

$\pi$  is a learnable projection function,  $\pi : \Phi \rightarrow \Psi^I$ , projecting the image representation of the classifier  $\Phi(x)$  to the VLR space,  $\Psi(x)$ , where  $x \in \mathcal{D}_{train}$ .  $\mathcal{D}_{train}$  denotes the training set. We follow (Moayeri et al., 2023) to learn  $\pi$ . Specifically,  $\pi$  is an affine transformation, *i.e.*,  $\pi_{W,b}(z) = W^T z + b$ , where  $W$  and  $b$  are the learnable weights and biases of the projector  $\pi$ . To retain the original semantics in the classifier representation space, we optimize the following objective:

$$W, b = \arg \min_{W, b} \frac{1}{|\mathcal{D}_{train}|} \sum_{x \in \mathcal{D}_{train}} \|W^T \Phi(x) + b - \Psi(x)\|_2^2 \quad (1)$$

### A.5 Precision@k

**Precision@k** (Eyuboglu et al., 2022; Yenamandra et al., 2023) measures the degree to which the predicted slices overlap with the ground truth slices in a dataset.

Let  $S = \{s_1, s_2, \dots, s_l\}$  represent the ground truth bias-conflicting slices in a dataset  $\mathcal{D}$ . A slice discovery algorithm  $A$  predicts a set of slices  $\hat{S} = \{\hat{s}_1, \hat{s}_2, \dots, \hat{s}_m\}$ . For each predicted slice  $\hat{s}_j$ , let  $O_j = \{o_{j1}, o_{j2}, \dots, o_{jn}\}$  denote the sequence of sample indices ordered by the decreasing likelihood that each sample belongs to the predicted slice  $\hat{s}_j$ .

Given a ground truth slice  $s_i$  and a predicted slice  $\hat{s}_j$ , we compute their similarity as:

$$P_k(s_i, \hat{s}_j) = \frac{1}{k} \sum_{i=1}^k \mathbb{I}[x_{o_{ji}} \in s_i],$$

where  $P_k(s_i, \hat{s}_j)$  is the proportion of the top  $k$  samples in the predicted slice  $\hat{s}_j$  that overlap with the samples in the ground truth slice  $s_i$ , and  $\mathbb{I}$  is an indicator function that returns 1 if the sample belongs to  $s_i$  and 0 otherwise.

For each ground truth slice  $s_i$ , we map it to the most similar predicted slice  $\hat{s}_j$  by maximizing  $P_k(s_i, \hat{s}_j)$ . We then compute the average similarity score between the ground truth slices and their best-matching predicted slices. Specifically, the Precision@k for a slice discovery algorithm  $A$  is given by:

$$\text{Precision@k}(A) = \frac{1}{l} \sum_{i=1}^l \max_{j \in [m]} P_k(s_i, \hat{s}_j),$$

where  $l$  is the number of ground truth slices,  $m$  is the number of predicted slices, and  $P_k(s_i, \hat{s}_j)$  is the similarity score for the ground truth slice  $s_i$  and predicted slice  $\hat{s}_j$ .

This metric evaluates how well the algorithm’s predicted slices match the bias-conflicting slices in the dataset, with higher scores indicating better alignment between predicted and ground truth slices. By computing the Precision@k, we can assess the effectiveness of slice discovery algorithms in identifying and isolating the most significant bias-conflicting regions in the data.

### A.6 CLIP Score

Kim et al. (2024) introduces the CLIP score, a metric that leverages the similarity between language and vision embeddings to quantify the influence of specific attributes on misclassified samples. In their method, attributes frequently present in misclassified images receive a high CLIP score, while absent ones score lower. For instance, in the Waterbirds dataset, the CLIP score for "bamboo" is high, as many misclassified waterbirds appear with bamboo in the background.

We propose a modification to the CLIP score. As discussed in Sec. 3.1, our goal is to identify visual attributes that are prevalent in correctly classified samples but absent in misclassified ones. This approach provides deeper insights into the attributes contributing to correct classifications, which is particularly valuable for medical images. In scenarios such as pneumothorax detection in the NIH dataset, understanding biases incorrectly classified cases—such as the presence of chest tubes—can help isolate features that lead to reliable diagnoses while addressing spurious correlations. Formally

we define the CLIP score corresponding to the attribute `attr` and a dataset  $\mathcal{D}$  as,

$$s_{CLIP}(\text{attr}, \mathcal{D}) = \text{sim}(\text{attr}, \mathcal{D}_{correct}) - \text{sim}(\text{attr}, \mathcal{D}_{wrong}),$$

where `attr` is the attribute obtained from the specific hypothesis by LLM, described in Sec. 3.2,  $\mathcal{D}_{correct}$  and  $\mathcal{D}_{wrong}$  are the correctly classified and misclassified samples. Also,  $\text{sim}(\text{attr}, \mathcal{D})$  is the similarity between the attribute `attr` and the dataset  $\mathcal{D}$ , estimated as the average cosine similarity between normalized embedding of a word  $\Psi^T(\text{attr})$  and images  $\Psi^I(x)$  for  $x \in \mathcal{D}$ , where

$$\text{sim}(\text{attr}, \mathcal{D}) = \frac{1}{|\mathcal{D}|} \sum_{x \in \mathcal{D}} \Psi^I(x) \Psi^T(\text{attr})$$

Refer to Appendix A.12.6 for the results.

### A.7 Prompts used by LLM for hypotheses generation

The following is a general template of the prompt utilized to generate the hypotheses from LLM, discussed in Sec. 3.2. In this template, we substitute the `<task>` placeholders with bird species, hair color, animal species, pneumothorax, cancer, and abnormality based on the corresponding dataset – Waterbirds, CelebA, MetaShift, NIH, RSNA-Mammo, and VinDr-Mammo. The modalities are natural images, chest-x-rays, and 2D mammograms. **Crucially, we only replace these two placeholders. We never include the actual dataset names or words like “water”, “land”, “gender”, “tube”, “background” or any other attributes leading to model’s mistakes in the prompt, as these may bias the LLM’s output.** For medical images, we also add: Ignore ‘\_\_\_’ as they are due to anonymization. We focus only on positive `<disease>` patients, as many reports consist of ‘\_\_\_’ for clarity. top `<K>` depends on the dataset discussed in the experiment section (Sec. 4).



## Prompt for Hypothesis Generation

**Context:** <task> classification from <modality> using a deep neural network.

**Analysis Post-Training:** On a validation set:

- a. Get the difference between the image embeddings of correct and incorrectly classified samples to estimate the features present in the correctly classified samples but missing in the misclassified samples.
- b. Retrieve the top <K> sentences from the <captions/radiology report> that match closely to the embedding difference in step a.
- c. The sentence list is given below:

TopK Sentence List

**Retrieved using Sec. 3.1**

These sentences represent the features present in the correctly classified samples but missing in the misclassified samples.

**Task:** Consider the consistent attributes present in the descriptions of correctly classified and misclassified samples regarding <task>. Formulate hypotheses based on these attributes. Attributes include all concepts (e.g., explicit or implicit anatomies, observations, symptoms of change related to the disease, concepts leading to potential bias in medical images, or visual cues in natural images) in the sentences. Assess how these characteristics might influence the classifier's performance.

Your response should only contain the list of top hypotheses, formatted as follows:

```
hypothesis_dict = {
  'H1': 'The classifier is making mistake as it is biased toward <attribute>',
  'H2': 'The classifier is making mistake as it is biased toward <attribute>',
  'H3': 'The classifier is making mistake as it is biased toward <attribute>',
  ...
}
```

To effectively test Hypothesis 1 (H1) using the CLIP language encoder, create prompts explicitly validating H1. These prompts will help generate text embeddings that capture the essence of the hypothesis, which can be compared with the image embeddings from the dataset. The goal is to verify alignment with or violation of H1. Prompts must focus only on the <task>. Each hypothesis must have five prompts, formatted as:

```
prompt_dict = {
  'H1_<attribute>': [List of prompts],
  'H2_<attribute>': [List of prompts],
  ...
}
```

Final response format strictly:

```
hypothesis_dict
prompt_dict
```

Table 3: Detailed description of the prompt for hypothesis generation and analysis for the <task> classification problem.

## A.8 Prompts and details on the experiments in RQ5 with instruction-tuned models (e.g., LLaVA)

In this setup, we don't use CLIP as VLR for the retrieval step discussed in Sec. 3.1. Instead, using the instruction-tuned vision language models (LLaVA-1.5 7B for natural images; cheXagent and RaDialog for CXRs), we first select the correctly classified images by the classifier  $f$ . Next, for each of the images, we pass them through the vision encoder in LLaVA and use the prompt for the natural images: "Describe the image" for the language model in LLaVA. For NIH, we use the prompt:

```
You are a radiologist. Based on the provided Chest X-Ray image and generate a structured report. The report should include sections for 'Findings,' 'Impression,' and 'Recommendations,' emphasizing relevant findings like consolidation, effusion, cardiomegaly, pneumonia, or pneumothorax. Use a formal radiology reporting style.
```

We select the texts for all the correctly classified images and follow LADDER's pipeline discussed in Sec 3.2 to generate the hypothesis (results shown in Fig. 5). Finally, we utilize LADDER's mitigation strategy, discussed in Sec. 3.3 to mitigate the biases (results shown in Tab. 6). **Note: in this experiment, we did not use any language explicitly. However, there is always a trade-off between getting language or using an instruction-tuning model like LLaVA.**

## A.9 Prompts and examples of metadata for detecting biases beyond radiology reports in RQ6

Refer to Tab. 4 for the prompt and the example of Python dictionary of metadata details of the correctly classified cancer patients to detect biases using LADDER.

## A.10 Extended details on general experiments

### A.10.1 Implementation details of the source model $f$ using ERM

For natural images and chest X-rays (CXRs), we resize the images to  $224 \times 224$  and train ResNet-50 (RN)(He et al., 2016) and Vision Transformer (ViT)(Dosovitskiy et al., 2020) models as  $f$  to predict labels. We explore various pretraining methods for initializing model weights, including supervised learning (Sup), SIMCLR(Chen et al., 2020), Barlow Twins (Zbontar et al., 2021),

DINO (Caron et al., 2021), and CLIP-based pre-training (Radford et al., 2021). The pretraining datasets utilized include ImageNet-1K (IN1)(Deng et al., 2009), ImageNet-21K (IN-21K)(Ridnik et al., 2021), SWAG (Singh et al., 2022), LAION-2B (Schuhmann et al., 2022), and OpenAI-CLIP (OAI) (Radford et al., 2021). For instance, "RN Sup IN1k" refers to a ResNet model pretrained using supervised learning and ImageNet-1K.

We train both ResNet and ViT models as  $f$  for natural images and NIH-CXR following the setup in Yang et al. (2023)<sup>4</sup>. Preprocessing steps include resizing the images to  $224 \times 224$ , applying center-cropping, and normalizing the images using ImageNet channel statistics. Consistent with prior work (Guo et al., 2020, 2019), we apply stochastic gradient descent (SGD) with momentum for optimization across all image datasets. Each model is trained for a total of 30,000 steps across all datasets, with specific training on Waterbirds and MetaShift for 5,000 steps each. For NIH, we utilize the Adam optimizer with a learning rate of 0.0001 and train for 60 epochs to achieve optimal convergence.

For RSNA-Mammo, we leverage the setting from one of the leading Kaggle competition solutions<sup>5</sup>. In this setup, the images are resized to  $1520 \times 912$ , and we train an EfficientNet-B5 model (Tan and Le, 2019) for 9 epochs using the SGD optimizer, with a learning rate of  $5e-5$  and a weight decay of  $1e-4$ .

Additionally, for CXR-CLIP, we use their pre-trained models<sup>6</sup>, which were trained on MIMIC-CXR and CheXpert (MC) datasets. For Mammo-CLIP, we utilize their EN-B5 variant<sup>7</sup>.

### A.10.2 Ablations

For the captioning ablations, we compare the performance of LADDER using BLIP (Li et al., 2022), BLIP-2 (Li et al., 2023a), ClipCap (Mokady et al., 2021), and GPT-4o (Wu et al., 2024). Additionally, for LLMs, we compare the performance of LADDER with GPT-4o (Wu et al., 2024), Claude 3.5 Sonnet, Llama 3.1 70B (Dubey et al., 2024), and Gemini 1.5 Pro (Team et al., 2024).

<sup>4</sup><https://github.com/YyzHarry/SubpopBench>

<sup>5</sup><https://github.com/Masaaaato/RSNABreast7thPlace>

<sup>6</sup><https://github.com/kakaobrain/cxr-clip>

<sup>7</sup><https://huggingface.co/shawn24/Mammo-CLIP/blob/main/Pre-trained-checkpoints/b5-model-best-epoch-7.tar>

**Context:** Breast cancer classification from mammograms using a deep neural network  
**Analysis post-training:** On a validation set, you are provided with the metadata details for the correctly classified positive cancer patients in a Python dictionary, as follows

#### Metadata Dictionary (Sample Entries)

- **Patient 1:** {site\_id: 1, laterality: L, view: MLO, age: 71, biopsy: 1, invasive: 1, BIRADS: 0, implant: 0, density: B, machine\_id: 49, photometric\_interpretations: Monochrome 1, voi\_lut\_function: SIGMOID, pixel\_intensity\_relationship: LOG}
- **Patient 2:** {site\_id: 2, laterality: L, view: CC, age: 83, biopsy: 0, invasive: 0, BIRADS: 0, implant: 1, density: D, machine\_id: 49, photometric\_interpretations: Monochrome 1, voi\_lut\_function: SIGMOID, pixel\_intensity\_relationship: LOG}
- ... (Additional metadata entries omitted for brevity)

**Task:** Consider the consistent attributes present in the dictionary regarding the positive cancer patients. Formulate hypotheses based on these attributes. Assess how these characteristics might be influencing the classifier’s performance. Your response should contain only the list of top hypothesis, nothing else. For the response, you should be the following python dictionary template, no extra sentence:

```
hypothesis_dict = {
  'H1': 'The classifier is making mistake as it is biased toward <attribute>',
  'H2': 'The classifier is making mistake as it is biased toward <attribute>',
  'H3': 'The classifier is making mistake as it is biased toward <attribute>',
  ...
}
```

Table 4: Prompts and examples of metadata for detecting biases beyond radiology reports in the experiment RQ6.

### A.10.3 Radiology text synthesis for 2D Mammograms

In Ghosh et al. (2024), the authors generate mammography reports using labeled mammographic attributes from the VinDr dataset in collaboration with a board-certified radiologist. This approach leverages the templated nature of breast mammogram reports, which are more standardized than those for other medical imaging modalities. This standardized structure follows protocols like BI-RADS (Breast Imaging-Reporting and Data System), which promotes uniformity in reporting (Palanisamy et al., 2023). Specifically, they focus on the following attributes: mass, architectural distortion, calcification, asymmetry (focal, global), density, suspicious lymph nodes, nipple retraction, skin retraction, and skin

thickening. Then they follow the report templates with radiologist-defined prompts in Ghosh et al. (2024), describing key parameters such as:

**Attribute Value:** Positive, negative, etc.

**Subtype:** Suspicious, obscured, spiculated, etc.

**Laterality:** Left or right breast.

**Position:** Upper, lower, inner, outer quadrant.

**Depth:** Anterior, mid, or posterior.

Finally, they generate concise report-like sentences by substituting these values into the templates. The authors leverage these sentences in Mammo-FActOR to perform weakly supervised localization of mammographic findings. In our work, we collect all these sentences to probe the EN-B5 classifier  $f$ , analyzing its errors during the retrieval step (Sec. 3.1) for the RSNA-Mammo and VinDr-Mammo datasets.

Below are some examples of mammography re-

1454 port sentences corresponding to the specific mam-  
1455 mographic attributes.

1456 **Mass:**

- 1457 1. there is a mass in the right breast  
1458 2. there is a mass in the right breast at  
1459 anterior depth  
1460 3. there is a mass in the upper right breast  
1461 at mid-depth  
1462 ...  
1463

1465 **Architectural distortion:**

- 1466 1. there is architectural distortion in the  
1467 right breast  
1468 2. there is architectural distortion in the  
1469 right breast at anterior depth  
1470 3. there is architectural distortion in the  
1471 right breast at mid-depth  
1472 ...  
1473

1475 **Calcification:**

- 1476 1. there is calcification in the right breast  
1477 2. there is calcification in the right  
1478 breast at anterior depth  
1479 3. there is calcification in the right  
1480 breast at mid depth  
1481 ...  
1483

1484 **Asymmetry:**

- 1485 1. there is a developing asymmetry in the  
1486 outer right breast  
1487 2. there is an asymmetry in the inner right  
1488 breast at anterior depth  
1489 3. there is an asymmetry in the right breast  
1490 at mid-depth  
1491 ...  
1493

1494 **Global Asymmetry:**

- 1495 1. there is a global asymmetry in the right  
1496 breast  
1497 2. there is a new global asymmetry in the  
1498 right breast  
1499 3. there is a global asymmetry in the inner  
1500 right breast  
1501 ...  
1503

1504 **Focal Asymmetry:**

- 1505 1. there is a focal asymmetry in the right  
1506 breast  
1507 2. there is a focal asymmetry in the right  
1508 breast at anterior depth  
1509 3. there is a focal asymmetry in the right  
1510 breast at mid depth  
1511 ...  
1513

1514 **Density:**

- 1515 1. the breasts being almost entirely fatty  
1516 2. scattered areas of fibroglandular density  
1517 3. the breast tissue is heterogeneously dense  
1518 4. the breasts are extremely dense  
1519 ...  
1520

1522 **Suspicious lymph node:**

- 1523 1. there is a suspicious lymph node in the  
1524 right axilla  
1525 2. there is a hyperdense lymph node in the  
1526 right axillary tail  
1527 3. there is an increased lymph node in the  
1528 right axillary tail  
1529 ...  
1530

1532 **Suspicious lymph node:**

- 1533 1. there is a suspicious lymph node in the  
1534 right axilla  
1535 2. there is a hyperdense lymph node in the  
1536 right axillary tail  
1537 3. there is an increased lymph node in the  
1538 right axillary tail  
1539 ...  
1540

1542 **Nipple retraction:**

- 1543 1. there is a new nipple retraction in the  
1544 right breast  
1545 2. there is an increased nipple retraction  
1546 in the right breast  
1547 3. there is a possible nipple retraction in  
1548 the right breast  
1549 ...  
1550

1552 **Skin retraction:**

- 1553 1. there is skin retraction in the right  
1554 breast  
1555 2. there is skin retraction in the inner  
1556 right breast  
1557 3. there is skin retraction in the lower  
1558 right breast  
1559 ...  
1560

1562 **Skin thickening:**

- 1563 1. there is increasing skin thickening of  
1564 the periareolar right breast  
1565 2. there is asymmetric skin thickening of  
1566 the lower right breast  
1567 3. there is asymmetric skin thickening of  
1568 the inner right breast  
1569 ...  
1570

1572 **A.11 Toy dataset construction**

1573 We construct a synthetic dataset based on the **CUB-**  
1574 **200-2011** (Wah et al., 2011) dataset, classifying  
1575 bird species into two categories: **Class 0** ( $y = 0$ )  
1576 and **Class 1** ( $y = 1$ ). Class 1 consists of the fol-  
1577 lowing bird species: *Albatross, Auklet, Cormorant,*  
1578 *Frigatebird, Fulmar, Gull, Jaeger, Kittiwake, Peli-*  
1579 *can, Puffin, Tern, Gadwall, Grebe, Mallard, Mer-*  
1580 *ganser, Guillemot, and Pacific Loon.* All remaining  
1581 bird species are assigned to Class 0. To introduce  
1582 spurious correlations, we overlay two 3D boxes  
1583 on each image. In the training set for Class 0, the  
1584 majority of samples (95%) were biased, with the  
1585 yellow box consistently placed to the left of the red  
1586 box. For Class 1, the boxes were randomly placed,

introducing variability in their positioning. In the validation and test sets, we split the positioning evenly, with 50% biased and 50% random samples across both classes, ensuring a balanced evaluation of the model’s reliance on spurious cues.

The primary goal of this dataset is to introduce a form of *reasoning* beyond the mere presence or absence of spurious correlations. Unlike prior datasets that rely on background cues (*e.g.*, Waterbirds or Metashift) or attributes like gender (*e.g.*, CelebA), our dataset integrates positional reasoning. Specifically, for Class 0, the yellow box is consistently placed to the left of the red box, creating a spurious correlation. For Class 1, the boxes are randomly positioned, removing this shortcut. The relative positioning of the boxes allows the captions to encode spatial relationships, which can be consumed by large language models (LLMs) to reason about these spatial cues. We train an ImageNet pretrained-ResNet model (RN Sup IN1k) on this dataset. Predictably, the classifier latches onto the spurious correlation of rectangle position, leading to underperformance on subsets where the shortcut is absent. The model achieves a mean accuracy of 85.6% and a worst-group accuracy (WGA) of 65.2%.

To analyze the model’s errors, we generate a corpus of rich captions for the validation set using a GPT-4o-based captioner. These captions describe both the presence of the rectangle and its position relative to the bird. Using LADDER, we aim to detect the reason for the classifier’s mistakes and mitigate it. LADDER leverages the reasoning capabilities of LLMs to capture both the presence of the rectangles and their relative spatial position. In contrast, methods *e.g.*, PRIME, rely on external tagging models, which only detect the presence or absence of shortcuts. Furthermore, since LADDER discovers biased attributes via LLM-generated reasoning, it can effectively mitigate these biases without requiring ground truth annotations or prior knowledge of the attributes.

The data is split into training, validation, and test sets, with all metadata (including labels, rectangle positions) saved for future analysis.

## A.12 Extended main results

### A.12.1 Results on WGA for using all slice discovery methods:

Fig.12 shows that LADDER improves WGA compared to other slice discovery methods for natural

images and CXRs. In this experimental setup, we first discover the slices with Domino (Eyuboglu et al., 2022), Facts (Yenamandra et al., 2023) and LADDER’s hypothesis-driven approaches. Next, we apply LADDER’s mitigation approach for each discovered slice to mitigate the biases and compute the WGA for each slice discovery method. As LADDER detects the slices precisely, it achieves better WGA compared to Domino and Facts. Fig. 13 shows LADDER improves WGA compared to other slice discovery methods for RSNA-Mammo and VinDr-Mammo datasets.

### A.12.2 Closest hypothesis to the ground truth attribute

Tab. 6 and Tab. 5 show the top3 hypotheses for RN Sup IN1K (convolution-based) and ViT Sup IN1K (transformer-based) architectures, respectively. These hypotheses are the most similar to the ground truth attribute on which the source model  $f$  is biased.

Table 5: Top 3 associated hypotheses for the ground truth biased attribute for ViT Sup IN1K model on various datasets

Dataset (Label)	Attribute	Top 3 hypotheses
Waterbirds (waterbird)	Water	1. activities like swimming or flying 2. conditions like cloudy or sunny 3. presence of objects like boats or rocks
Waterbirds (landbird)	Land	1. bird in the middle of a forest 2. yellow bird 3. bird sitting on top of a tree
CelebA (Blonde)	Women	1. woman wearing red dress 2. woman with red top 3. black jacket
MetaShift (Dog)	Outdoor	1. presence of a leash 2. presence of a ball 3. presence of a car
MetaShift (Cat)	Indoor	1. beds 2. windows 3. televisions

### A.12.3 Extended qualitative results for our slice discovery method on various datasets

Figures 24 and 19 report LLM-generated the list of hypotheses and the prompts to test them discussed in the Sec. 5. Figures 20, 21, 22, 23, and 25 illustrate qualitative results of our method applied on various datasets using RN Sup IN1k models. Specifically, they showcase the classification of pneumothorax patients from NIH, “landbird” from the Waterbirds, “blond” from CelebA, “cat” and “dog” from MetaShift, and “cancer” from the RSNA-Mammo datasets, respectively. In all the cases, LADDER correctly identifies the hypothesis with true attribute causing biases in the given classifier  $f$ .



**Extracted hypotheses by Ladder**  
 The classifier is making mistake as it is biased toward:  
**H1:** relative positioning of red and yellow box  
**H2:** images with small birds  
**H3:** images with overlapping boxes  
**H4:** the position of boxes relative to the bird  
**H5:** images with bird on branches

Figure 11: Sample images of our toy dataset to validate the reasoning of LLM utilized by LADDER. The dataset has two classes. Images with class 0 are biased, with the yellow box always placed to the left of the red box. For images with class 1, the boxes are randomly placed.

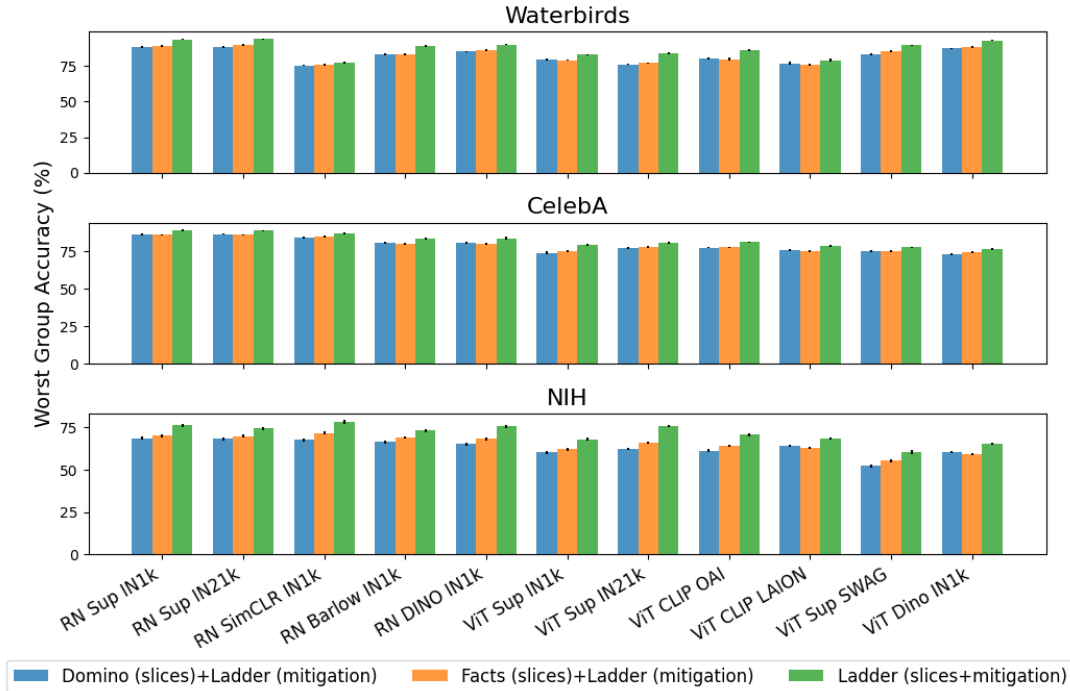


Figure 12: LADDER slices consistently outperform those from Domino and Facts when combined with LADDER’s bias mitigation strategy across various settings.

#### A.12.4 Comparing the performance of LADDER for error mitigation across architectures

Tab. 8 compares LADDER with additional bias mitigation baselines for CNN-based models. Tab. 9 compares different error mitigation algorithms for ViT Sup IN1K-based models ( $f$ ), for all the SOTA mitigation baselines discussed in Appendix A.3. For natural images (Waterbirds and CelebA), we report mean accuracy. For medical images (NIH, RSNA and VinDr), we report mean AUROC. Fig. 15 reports the WGA and shows that LADDER outperforms the other slice discovery baselines across the different architectures and pre-training strategies.

#### A.12.5 Application: Improvement on the zero-shot accuracy of Vision Language models using the attributes from the extracted hypothesis by LADDER

To evaluate the impact of LADDER’s attribute-based slice discovery on zero-shot performance, we conducted experiments using a CLIP-based vision-language model across multiple datasets. LADDER extracts fine-grained attributes from error-prone data slices, which we incorporated as detailed prompts for zero-shot classification. These prompts were generated from hypotheses produced by the LADDER framework and reflect nuanced characteristics of the data that a model might otherwise overlook. We compare these attribute-driven prompts against standard, baseline prompts typically used for zero-shot tasks.

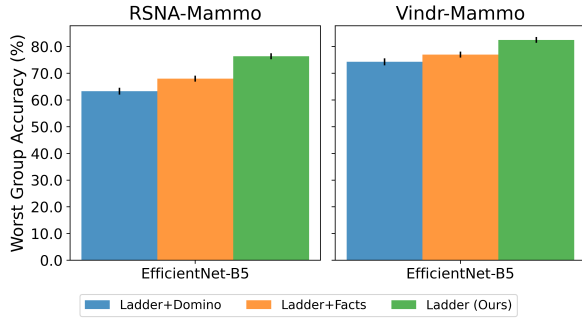


Figure 13: LADDER improves WGA compared to other bias mitigation methods for RSNA-Mammo and VinDr-Mammo datasets.

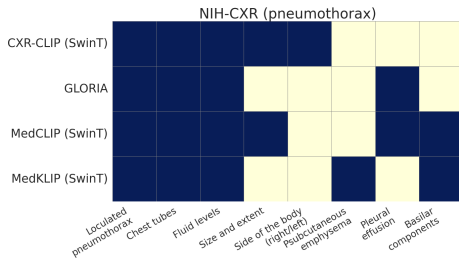


Figure 14: Effect of different VLRs for CXRs on biased attribute discovery by LADDER. Bright/light colors denote presence/absence of the attributes.

**Experimental Process.** For each dataset, we implemented two types of zero-shot prompts:

- **Baseline prompts:** CLIP-based prompts (Radford et al., 2021) e.g., [a photo of a landbird and a photo of a waterbird] for the Waterbirds dataset for natural images, CXR-CLIP (You et al., 2023) prompts e.g., [no pneumothorax, pneumothorax] for NIH, Mammo-CLIP (Ghosh et al., 2024) prompts e.g., [{no cancer, no malignancy}, {cancer, malignancy}] for RSNA-Mammo and VinDr-Mammo.
- **LADDER-derived prompts:** These prompts were generated based on the attributes extracted from LADDER’s hypotheses, providing a more detailed description of the data. For example, in the Waterbirds dataset, we used prompts like a photo of a waterbird on docks and boats or a photo of a landbird inside on bamboo forest. In this experiment, we use the attributes from the hypotheses extracted from RN Sup IN1k (Resnet 50 pretrained with ImageNet 1K and supervised learning) classifier.

Table 6: Top 3 associated hypotheses for the ground truth biased attribute for RN Sup IN1K model on various datasets

Dataset (Label)	Attribute	Top 3 hypotheses
Waterbirds (waterbird)	Water	1. water bodies like oceans and lakes 2. actions like flying or sitting 3. conditions, e.g., cloudy skies
Waterbirds (landbird)	Land	1. bird being in flight 2. bird perching on top of a tree 3. bird perching on a tree branch
CelebA (Blonde)	Women	1. woman with long hair 2. woman wearing red dress 3. a black jacket
MetaShift (Dog)	Outdoor	1. dogs in motion 2. dogs on leashes 3. beach environments
MetaShift (Cat)	Indoor	1. televisions 2. windows 3. beds
NIH (pneumothorax)	Chest tube	1. the presence of chest tubes 2. localized pneumothorax 3. size and extent of pneumothorax
RSNA-Mammo (cancer)	Calcification	1. scattered calcifications 2. vascular calcifications 3. bilateral occurrences

Table 7: **Token Usage and Cost for Each LLM.** Each row shows the breakdown for an LLM extracting hypotheses across all 6 datasets, using RN Sup IN1k (natural images / CXRs) and EN-B5 (mammograms).

Model Name	Input Tokens	Output Tokens	Total Cost
GPT-4o	33,217	4,284	\$2.51
Claude 3.5 Sonnet	34,888	4,473	\$0.17
Gemini 1.5 Pro	33,872	4,378	\$0.32
Llama 3.1 70B	32,688	4,176	\$0.05
<b>Total</b>	<b>134,665</b>	<b>17,311</b>	<b>\$3.05</b>

We evaluated the zero-shot classification performance of the model using both prompt types. The results are shown in Tab. 10.

**Results.** The results demonstrate a significant improvement in zero-shot accuracy when using LADDER-extracted attributes as prompts. Across all datasets, the attribute-driven prompts outperformed the baseline, indicating the effectiveness of using detailed, hypothesis-driven attributes to enhance zero-shot performance. In the **Waterbirds** dataset, LADDER prompts improved accuracy by +8.56%, rising from 50.40% with baseline prompts to 58.96% with LADDER attributes. The improvement was even more pronounced for the **NIH** dataset, with a +19.05% gain (49.17% to 68.22%). The **RSNA** dataset also saw a notable improvement, with a +5.81% gain in accuracy (60.17% to 65.98%). The improvements for **CelebA** (+0.32%) and **VinDr** (+1.41%) were more modest but still indicate that using LADDER’s attribute-based prompts provides consistent gains across various domains. These results highlight the ability of LADDER to extract meaningful attributes that guide the vision-language model to

Table 8: Benchmarking error mitigation methods over 3 seeds for CNN models (EN-B5 for mammograms and RN Sup IN1k for the rest). For natural images (Waterbirds and CelebA), we report mean accuracy. For medical images (NIH, RSNA and VinDr), we report mean AUROC. We bold-face and underline the best and second-best results, respectively.

Method	Waterbirds		CelebA		NIH		RSNA		VinDr	
	Mean(%)	WGA(%)	Mean(%)	WGA(%)	Mean(%)	WGA(%)	Mean(%)	WGA(%)	Mean(%)	WGA(%)
Vanilla (ERM)	88.2±0.7	69.1±1.2	94.1±0.2	62.2±1.5	<b>87.4</b> ±0.0	60.3±0.0	<b>86.5</b> ±0.0	69.8±0.0	<b>86.9</b> ±0.0	45.6±0.0
Mixup	88.5±0.5	77.3±0.5	<u>94.5</u> ±0.1	57.8±0.8	85.1±0.0	67.6±0.8	84.5±0.0	64.8±0.0	83.2±0.0	65.3±0.0
IRM	88.1±0.2	74.3±0.1	<u>94.5</u> ±0.5	63.3±2.5	83.2±0.0	63.4±0.0	83.3±0.0	68.4±0.0	83.5±0.0	65.2±0.0
MMD	92.5±0.1	83.5±1.1	<u>92.5</u> ±0.6	22.7±2.5	84.6±0.0	65.4±0.0	84.2±0.0	69.1±0.0	81.2±0.0	64.8±0.0
Focal	89.3±0.2	71.6±0.8	<b>94.9</b> ±0.3	59.3±2.0	85.5±0.0	68.9±0.7	83.6±0.0	65.5±0.0	82.6±0.0	63.7±0.0
CBLoss	91.3±0.7	86.1±0.3	91.2±0.7	87.3±0.5	85.5±0.0	63.4±0.0	83.2±0.0	65.1±0.0	81.7±0.0	62.5±0.0
LDAM	91.3±0.7	86.1±0.3	<u>94.5</u> ±0.2	58.3±2.5	84.3±0.0	69.4±0.2	81.6±0.0	63.5±0.0	81.2±0.0	62.2±0.0
CRT	90.5±0.0	79.7±0.3	<u>92.5</u> ±0.1	87.3±0.3	82.7±0.0	68.5±0.0	82.7±0.0	68.8±0.0	82.9±0.0	63.3±0.0
ReWeightCRT	91.3±0.1	78.4±0.1	<u>92.5</u> ±0.2	87.2±0.5	83.0±0.0	69.5±0.0	82.4±0.0	68.3±0.0	82.9±0.0	63.3±0.0
JTT	88.8±0.7	84.5±0.3	90.6±2.2	87.2±7.5	85.1±0.0	70.4±0.0	84.6±0.0	68.5±0.0	83.7±0.0	66.1±0.0
GroupDRO	88.8±1.7	87.1±1.3	91.4±0.6	<u>88.1</u> ±0.7	85.2±0.0	71.1±0.0	85.1±0.0	72.3±0.0	82.7±0.0	67.1±0.0
CVaRDRO	89.8±0.4	85.4±2.3	<u>94.5</u> ±0.1	83.1±1.5	85.7±0.1	71.3±0.0	85.4±0.0	71.7±0.0	82.7±0.0	67.1±0.0
LfF	87.0±0.3	75.2±0.7	81.1±5.6	63.0±4.4	75.9±0.0	61.6±0.0	79.8±0.0	66.4±0.0	82.4±0.0	64.5±0.0
LISA	92.8±0.3	88.7±0.6	92.6±0.1	86.2±1.1	85.2±0.0	66.6±0.0	85.1±0.0	64.4±0.0	82.8±0.0	63.1±0.0
DFR	<u>92.3</u> ±0.2	88.2±0.3	89.3±0.2	87.1±1.1	86.1±0.0	70.5±0.0	85.1±0.0	71.2±0.0	83.8±0.0	68.1±0.0
<b>LADDER (ours)</b>	<b>93.1</b> ±0.8	<b>91.4</b> ±0.8	89.8±1.2	<b>88.9</b> ±0.4	<u>86.8</u> ±0.0	<b>76.2</b> ±0.0	<u>85.3</u> ±0.0	<b>76.4</b> ±0.0	<u>86.2</u> ±0.0	<b>82.5</b> ±0.0

Table 9: Benchmarking error mitigation methods over 3 seeds for ViT models pretrained with IN1k using the supervised method (RN Sup IN1k). We bold-face and underline the best and second-best results, respectively.

Method	Waterbirds		CelebA	
	Mean(%)	WGA(%)	Mean(%)	WGA(%)
Vanilla (ERM)	82.7±1.4	51.2±1.3	95.2±0.4	46.8±1.1
Mixup	81.8±0.4	44.9±0.3	<b>95.8</b> ±0.3	48.3±0.3
IRM	79.8±0.3	54.5±0.3	85.1±1.2	48.7±0.3
MMD	83.6±2.7	42.5±1.1	95.6±0.4	54.2±0.4
JTT	81.7±0.5	49.1±0.5	94.8±0.3	52.7±0.6
GroupDRO	82.2±0.8	53.1±1.2	93.5±0.1	80.1±0.4
CVaRDRO	83.5±0.3	46.6±2.8	95.6±0.1	55.1±1.8
LISA	83.7±0.1	48.8±0.1	95.6±0.2	60.2±0.1
DFR	85.0±0.3	76.2±0.3	91.3±1.1	81.1±0.5
<b>LADDER (ours)</b>	<b>85.3</b> ±0.5	<b>86.5</b> ±0.4	90.7±0.1	83.4±0.1

more accurate predictions, even in zero-shot settings where explicit training on the target data is absent. By leveraging these hypotheses, LADDER enables more precise alignment between image representations and class descriptions, significantly enhancing zero-shot performance.

### A.12.6 CLIP score comparison of various attributes extracted by LADDER

Refer to Fig. 16 for the CLIP scores (discussed in Appendix A.6) of various attributes extracted from the hypotheses by LADDER. For *e.g.*, the correctly classified samples for the waterbird class in the Waterbirds dataset have a bias on the water-related backgrounds. As a result, the CLIP score of ocean,

Table 10: Application: Boost in Zero-shot accuracy results using attributes from the hypotheses extracted from RN Sup IN1k (Resnet 50 pretrained with ImageNet 1K and supervised learning) classifier

Dataset	CLIP Prompts	LADDER Hypotheses	Gain
Waterbirds	50.40	<b>58.96</b>	+8.56 ↑
CelebA	86.69	<b>87.01</b>	+0.32 ↑
NIH	49.17	<b>68.22</b>	+19.05 ↑
RSNA	60.17	<b>65.98</b>	+5.81 ↑
VinDr	90.92	<b>92.33</b>	+1.41 ↑

boat, lake is high. We observe consistent results for other datasets as well.

### A.12.7 Improvement on different slices of UrbanCars benchmark

Tab. 11 shows that LADDER achieves higher accuracy compared to the Whac-A-Mole method (Li et al., 2023b) across multiple shortcut benchmarks on the Urbancars dataset, without prior knowledge of the number or types of possible shortcuts.

Table 11: LADDER achieves higher accuracy compared to the Whac-A-Mole method (Li et al., 2023b) across multiple shortcut benchmarks on the Urbancars dataset without prior knowledge of the number or types of possible shortcuts.

Method	Mean Acc	BG gap	CoObj Gap	BG+CoObj Gap
ERM	96.4	-15.3	-11.2	-69.2
Whac-A-Mole	95.2	-2.4	-2.9	-5.8
LADDER	92.2	-1.1	-1.6	-3.8



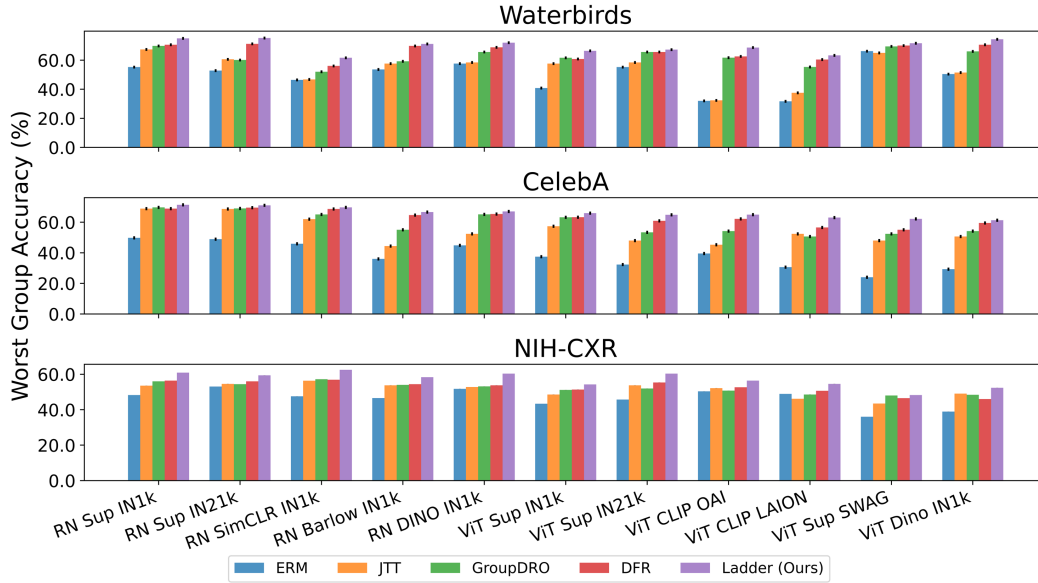


Figure 15: WGA across bias mitigation methods. LADDER consistently outperforms other bias mitigation baselines (ERM, JTT, GroupDRO, and DFR) across different model architectures and pre-training strategies.

### A.12.8 Extended results on discovered hypothesis by LADDER for various architectures and pre-training methods

Fig. 17 illustrates additional results for the CelebA and Metashift datasets, demonstrating that LADDER accurately captures various sources of bias, regardless of the underlying architectures or pre-training methods.

### A.12.9 Results on Imagenet

Tables 12, 13, 14 shows that LADDER identifies unique biases for the Imagenet dataset for a stethoscope, ant, and horizontal bar, respectively.

### A.12.10 Ablation 1: WGA of LADDER using other captioning methods

Tab. 1 presents an ablation study evaluating the effect of various captioning models on LADDER’s performance in mitigating biases. The quality of captions directly affects LADDER’s ability to effectively generate hypotheses, as these captions are analyzed by LLMs to identify biased attributes contributing to model errors. LADDER then pseudo-labels these attributes to systematically mitigate the identified biases. We consider different captioning models, including BLIP (Li et al., 2022), BLIP2 (Li et al., 2023a), ClipCap (Mokady et al., 2021), and GPT-4o (Wu et al., 2024), with ResNet Sup IN1k as the classifier.

The results indicate that the more advanced

captioning model, GPT-4o, significantly improves LADDER’s performance, achieving the highest Worst Group Accuracy (WGA) and mean accuracy across both datasets. Specifically, GPT-4o achieves a WGA of 94.5% on Waterbirds and 91.9% on CelebA, which is substantially better than the other models. BLIP and BLIP2 demonstrate comparable results, with BLIP slightly outperforming BLIP2 in the Waterbirds dataset, while BLIP2 performs better on CelebA in WGA. In contrast, ClipCap consistently yields the lowest scores, implying that simpler captioning methods are less effective for enhancing LADDER’s bias identification capabilities. Overall, the results underscore the importance of selecting a high-quality captioning model to maximize LADDER’s effectiveness. While more sophisticated models like GPT-4o entail higher costs, their significant impact on bias mitigation performance, particularly on WGA, makes them an indispensable choice in scenarios where accuracy is critical.

### A.12.11 Ablation 2: Slice discovery by LADDER using different LLMs

In this ablation study, we explore how different LLMs impact the effectiveness of LADDER in discovering data slices and generating hypotheses for bias identification. We aim to discover the biases from RN Sup IN1k classifier for natural images and CXRs, and EN-B5 classifier for mammograms. We utilize four LLMs: GPT-4o, Claude 3.5 Sonnet, LLaMA 3.1 70B, and Gemini 1.5 Pro. Fig. 18

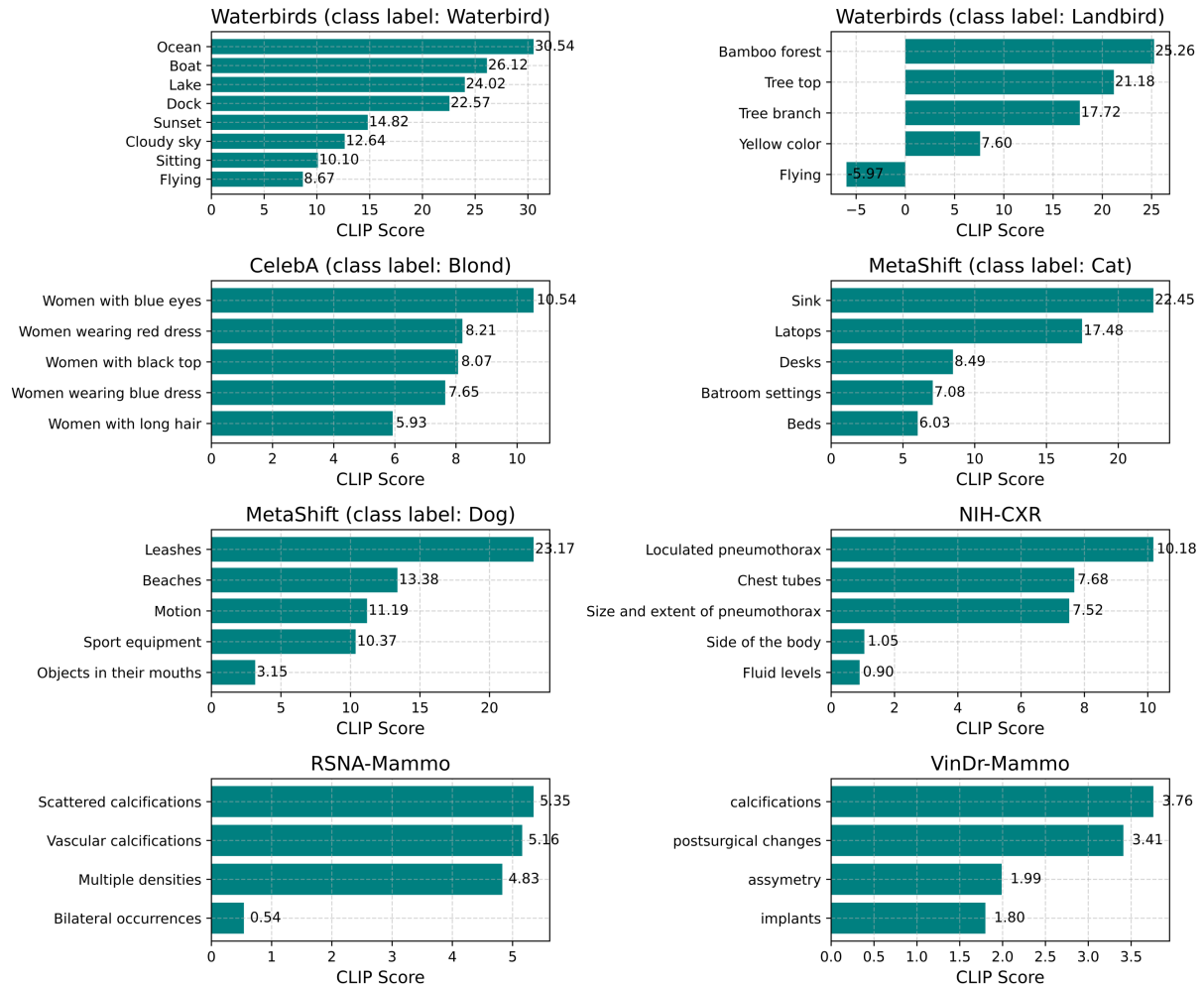


Figure 16: CLIP Score(Appendix A.6) for various attributes extracted from the hypotheses by LADDER. CLIP scores of the attributes are high signifying that they induce biases on the correctly classified samples.

1836 illustrates the different attributes these models high-  
 1837 light across multiple datasets, including Waterbirds,  
 1838 CelebA, NIH, RSNA, VinDr, and MetaShift. Each  
 1839 LLM aims to extract a hypothesis related to an at-  
 1840 tribute, signifying the classifier’s mistake. These at-  
 1841 tributes potentially lead to systematic model biases.  
 1842 As shown in Fig. 18, each LLM focuses on distinct  
 1843 subsets of attributes, reflecting their unique inter-  
 1844 pretation capabilities. Despite these differences,  
 1845 there is significant overlap in the overall hypothe-  
 1846 ses generated across the models, indicating consis-  
 1847 tency in identifying the attributes contributing to  
 1848 model errors.

1849 For instance, in the Waterbirds dataset, all LLMs  
 1850 frequently highlight attributes like ocean and boat  
 1851 for the waterbird class and bamboo forest and  
 1852 tree branch for the landbird class. These at-  
 1853 tributes align closely with the ground truth bias in  
 1854 this dataset, which relates to water and land back-  
 1855 grounds being associated with the respective bird

1856 classes. This suggests that LLMs effectively iden-  
 1857 tify these underlying environmental biases that lead  
 1858 to systematic errors. Similarly, in medical datasets,  
 1859 such as NIH-CXR for pneumothorax, all LLMs  
 1860 consistently highlight chest tube as a common  
 1861 attribute for misclassified samples. This reflects  
 1862 a true bias, as the presence of a chest tube often  
 1863 strongly correlates with pneumothorax cases. Identi-  
 1864 fying this attribute helps understand the systemat-  
 1865 ic bias that models may develop when chest tubes  
 1866 are spuriously correlated in pneumothorax images.

1867 This consistency across various LLMs demon-  
 1868 strates the robustness of LADDER for systematic  
 1869 bias detection, irrespective of the underlying LLM  
 1870 used. The results highlight that LADDER is effec-  
 1871 tive at leveraging the strengths of different LLMs  
 1872 to produce meaningful insights into model behav-  
 1873 ior, regardless of which LLM is utilized. More-  
 1874 over, it emphasizes the versatility of using LLMs  
 1875 for extracting domain-specific attributes—whether

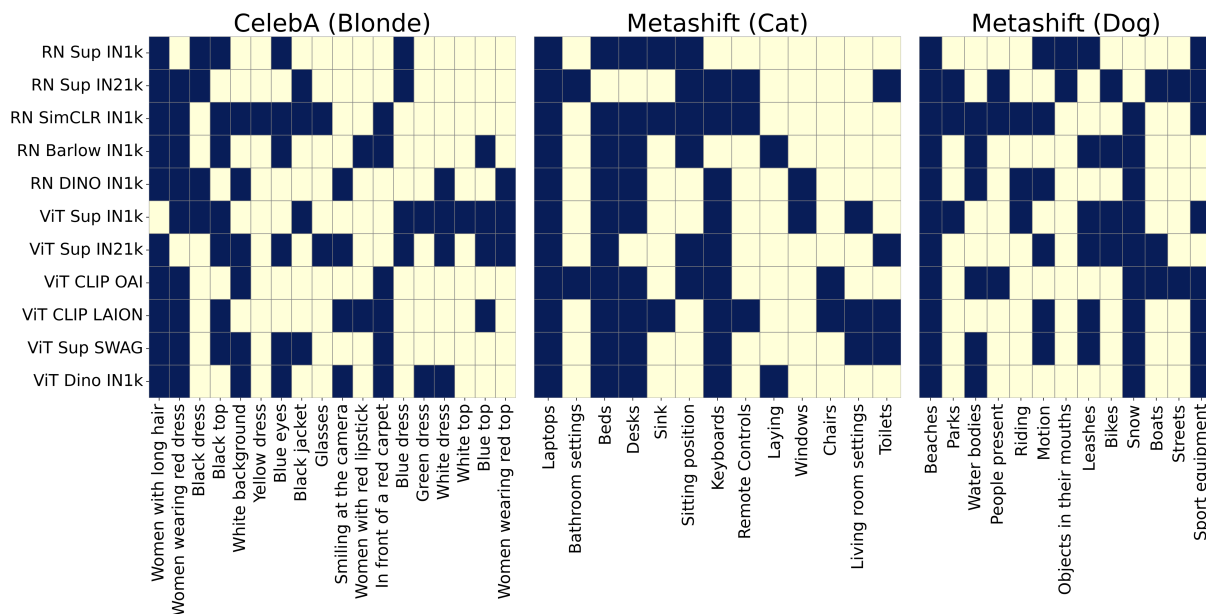


Figure 17: LADDER accurately captures various sources of bias, regardless of the underlying architectures or pre-training methods for the CelebA and Metashift datasets. Bright colors indicate attributes in LADDER’s hypotheses, while light colors indicate their absence.

the focus is on natural images, chest X-rays, or mammography scans – while maintaining cost efficiency and avoiding manual annotation. Overall, this ablation shows that the specific choice of LLM slightly influences which attributes are emphasized, but all models effectively support the generation of comprehensive hypotheses that capture the biases inherent in different datasets.

#### A.12.12 Ablation 3: WGA by LADDER using the hypothesis by different LLMs

Fig. 10 illustrates the worst group accuracy (WGA) achieved across multiple datasets when utilizing LADDER to mitigate biases with different LLMs. The LLMs compared in this study include Claude 3.5 Sonnet, LLaMA 3.1 70B, Gemini 1.5 Pro, and GPT-4o. We consider the RN Sup IN1k classifier for natural images and CXRs, as well as the EN-B5 classifier for mammograms. The primary aim of this ablation is to assess how well LADDER can mitigate biases when generating hypotheses using different LLMs. As shown in Fig. 10, the WGA values remain consistently high across all LLMs, indicating that LADDER is effective in mitigating biases irrespective of the choice of LLM for hypothesis generation. Specifically, all LLMs achieve WGA scores of over 80% for most datasets, with only slight variations between models. This consistency demonstrates the robustness of LADDER in leveraging different LLMs to address model bi-

ases effectively. For datasets like Waterbirds and CelebA, the performance across all LLMs is nearly identical, suggesting that the generated hypotheses successfully capture the underlying biases and lead to similar improvements in fairness. In medical datasets, such as NIH and RSNA, the trend is also maintained, with LLMs like GPT-4o and Gemini 1.5 Pro achieving better results than other LLMs. These findings emphasize that the specific choice of LLM has only a minor impact on the overall ability of LADDER to mitigate bias. This makes LADDER a flexible and cost-effective solution, as it can work effectively with a range of LLMs, each with different computational costs and capabilities. Using different LLMs ensures flexibility based on resource availability while effectively identifying and mitigating dataset biases.

#### A.12.13 Ablation 4: Overall cost and choice of LLMs

Tab. 7 shows the cost of using various LLMs. Each row shows the total breakdown for an LLM extracting hypotheses across all 6 datasets, using RN Sup IN1k (natural images or CXRs) and EN-B5 (mammograms). LADDER invokes LLM once using sentences only (no images). The total cost incurred is ~\$28 across all architectures and pretraining used in the experiments. Thus, LLMs are far more cost-effective than developing new tagging models for unexplored domains *e.g.*, radiology, or manually

1934 annotating shortcuts. Fig. 18 in Appendix A.12.11  
 1935 shows the attributes identified by each LLM while  
 1936 generating hypotheses. Different LLMs capture  
 1937 distinct sets of attributes, yet substantial overlap  
 1938 exists, with many attributes consistently revealing  
 1939 actual biases across models. Ablation studies in Ap-  
 1940 pendix A.12.12 indicate that using different LLMs  
 1941 to compute WGA shows that Gemini and GPT-4o  
 1942 achieve higher WGA for medical images than the  
 1943 others.

#### 1944 A.12.14 Ablation 5: Choice of VLR on 1945 LADDER

1946 Fig.14 demonstrates that LADDER consistently  
 1947 detects well-known biases in CXRs, such as  
 1948 chest tube, across various VLRs (CXR-CLIP  
 1949 (SwinT), GLORIA (Huang et al., 2021), Med-  
 1950 CLIP (SwinT) (Wang et al., 2022), and MedKLIP  
 1951 (SwinT) (Wu et al., 2023)) on the NIH dataset. This  
 1952 consistency suggests that the choice of VLR does  
 1953 not significantly impact LADDER’s ability to iden-  
 1954 tify biased attributes.

Table 12: LADDER identifies unique biases in **ImageNet** for the “Stethoscope” class. The table shows accuracy for subpopulations where the hypothesis failed (Error Slice) and where it passed (Bias-Aligned).

Biases	Accuracy of the subpopulation where hypothesis failed (Error Slice) (%)	Accuracy of the subpopulation where hypothesis passed (Bias-Aligned) (%)
Littmann branding	51.3	95.2
Dual-head stethoscopes	53.7	95.2
Medical settings	51.3	93.3
Colors <i>e.g.</i> , yellow or copper	55.6	87.8
Children interacting with stethoscopes	58.2	93.6

Table 13: LADDER identifies unique biases in **ImageNet** for the “Ant” class. The table shows accuracy for subpopulations where the hypothesis failed (Error Slice) and where it passed (Bias-Aligned).

Biases	Accuracy of the subpopulation where hypothesis failed (Error Slice) (%)	Accuracy of the subpopulation where hypothesis passed (Bias-Aligned) (%)
Close up settings	62.6	73.3
Textured surface	59.6	74.5
Green Leaves	67.5	76.5
Yellow flower	62.4	69.8
Black ant	63.8	73.1

Table 14: LADDER identifies unique biases in **ImageNet** for the “Horizontal bar” class. The table shows accuracy for subpopulations where the hypothesis failed (Error Slice) and where it passed (Bias-Aligned).

Biases	Accuracy of the subpopulation where hypothesis failed (Error Slice) (%)	Accuracy of the subpopulation where hypothesis passed (Bias-Aligned) (%)
Child	66.4	82.4
Playground	61.4	82.7
Green Leaves	67.7	76.5
Yellow flower	62.5	69.8
Black ant	63.5	73.8

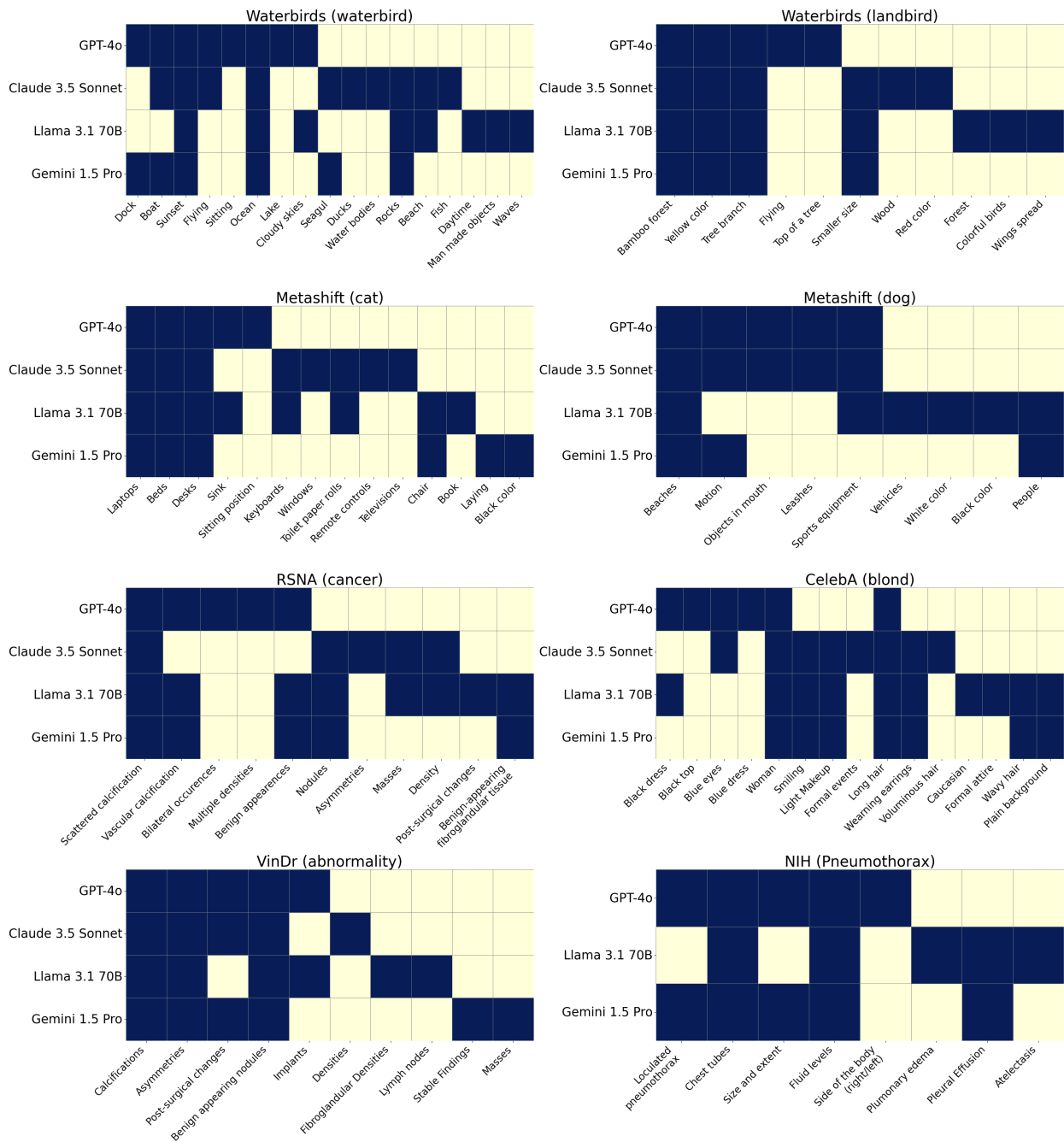


Figure 18: Ablation 2: Attributes identified by different LLMs while generating hypotheses across datasets for bias identification: RN Sup IN1k for natural images and CXRs, and EN-B5 for mammograms. Each LLM (GPT-4o, Claude 3.5 Sonnet, LLaMA 3.1 70B, Gemini 1.5 Pro) focuses on distinct attributes, yet the overall hypotheses are consistent across datasets, showing LADDER’s robust bias detection. Bright colors indicate attributes in LADDER’s hypotheses, while light colors indicate their absence. Following MIMIC’s regulations, we use Gemini 1.5 Pro (via Vertex AI on Google Cloud Platform), GPT-4o via Azure OpenAI service, and Llama 3.1 70B (running locally) for NIH. Bright colors indicate attributes in LADDER’s hypotheses.

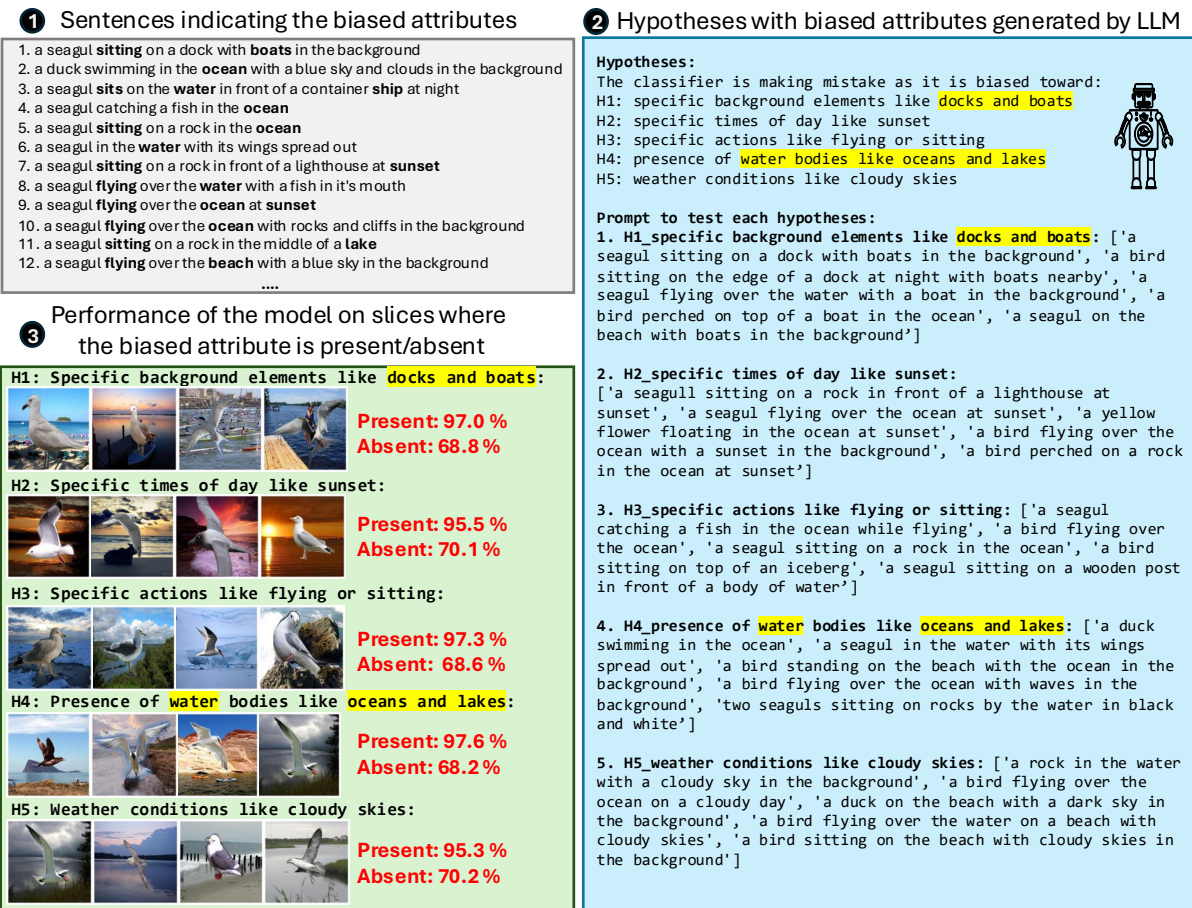


Figure 19: LADDER discovers slices for biased attributes in RN Sup IN1k-based classifier for *waterbird* classification in **Waterbirds** dataset. This figure details the slice discovery process for biased attributes involving sentence analysis, hypothesis generation by an LLM, and the model's performance on slices where attributes are present or absent, demonstrating how biases affect classifier accuracy. We highlight the hypothesis generated by LADDER that corresponds to the ground truth biased attribute (e.g., water for landbirds) in **yellow**.

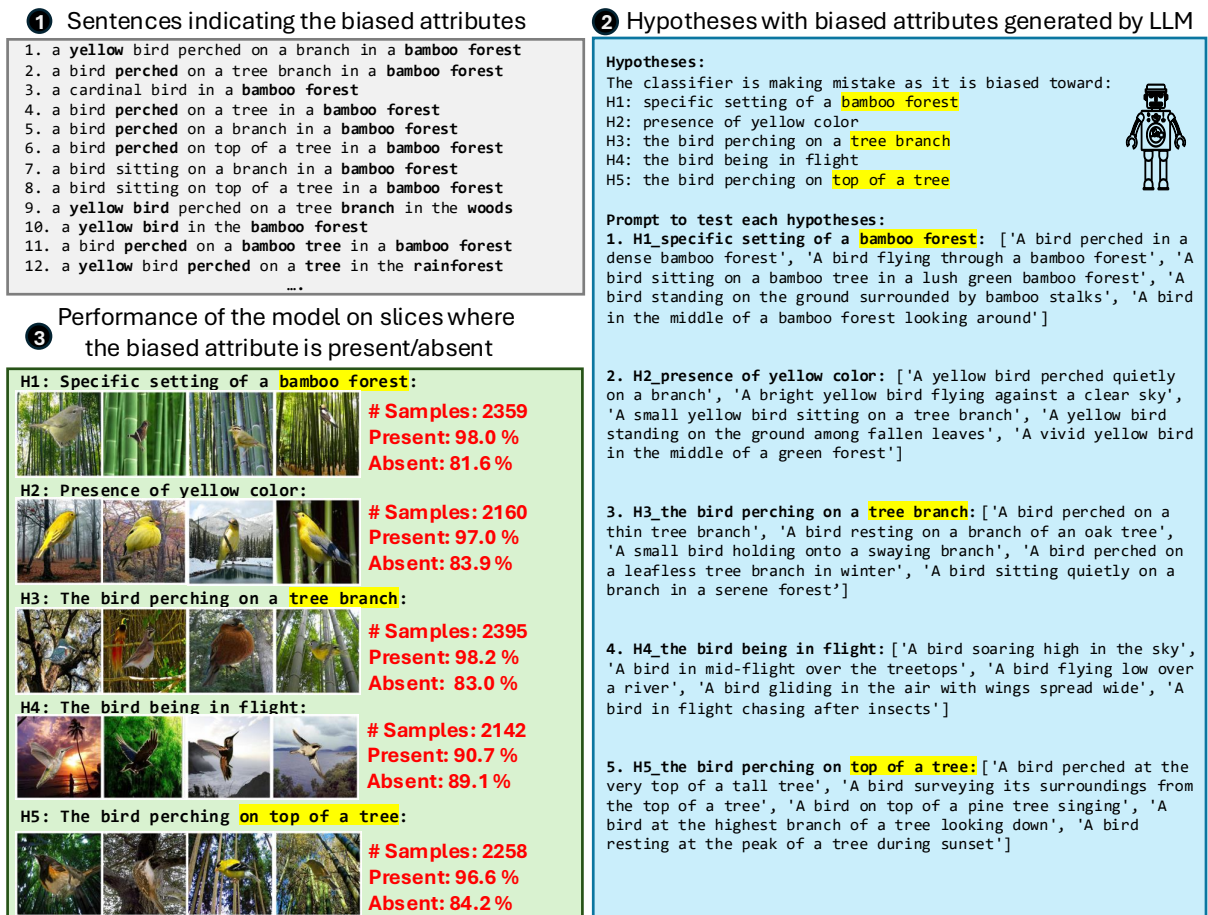


Figure 20: LADDER discovers slices for biased attributes in RN Sup IN1k-based classifier for *landbird* classification in **Waterbirds** dataset. This figure details the slice discovery process for biased attributes involving sentence analysis, hypothesis generation by an LLM, and the model’s performance on slices where attributes are present or absent, demonstrating how biases affect classifier accuracy. We highlight the hypothesis generated by LADDER that corresponds to the ground truth biased attribute (e.g., Land for landbirds) in **yellow**.

### 1 Sentences indicating the biased attributes

1. a woman with **long blonde** hair **smiling** and wearing a **black top**
2. a woman with **long blonde** hair standing in front of a **red carpet**
3. a woman with **long blonde** hair standing on a **red carpet**
4. a girl with **long blonde** hair in a black frame on a **white background**
5. a woman with **long blonde** hair standing in front of a **stone wall**
6. a woman with **long blonde** hair is smiling and holding a pillow
7. a woman with **long blonde** hair posing in front of a christmas tree
8. a woman with **long blonde** hair standing in front of a christmas tree
9. a woman with blonde hair standing on a **red carpet**
10. a woman with **long blonde** hair and **blue eyes smiles** at the camera
11. a woman with **long blonde** hair and a **black jacket smiles** at the camera
12. a woman with **long blonde** hair in front of a **white background**

### 3 Performance of the model on slices where the biased attribute is present/absent

<b>H1: black top:</b>		
		<b># Sample: 64</b> <b>Present: 99.4 %</b> <b>Absent: 59.5 %</b>
<b>H2: woman wearing a red dress:</b>		
		<b># Sample: 55</b> <b>Present: 98.0 %</b> <b>Absent: 80.1 %</b>
<b>H3: blue dress:</b>		
		<b># Sample: 57</b> <b>Present: 98.6 %</b> <b>Absent: 80.4 %</b>
<b>H4: woman with long hair:</b>		
		<b># Sample: 62</b> <b>Present: 97.8 %</b> <b>Absent: 79.5 %</b>
<b>H5: blue eyes:</b>		
		<b># Sample: 76</b> <b>Present: 99.2 %</b> <b>Absent: 78.7 %</b>

### 2 Hypotheses with biased attributes generated by LLM

#### Hypotheses:

The classifier is making mistake as it is biased toward:

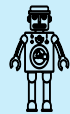
H1: black top

H2: **woman** wearing a red dress

H3: a blue dress

H4: **woman** with long hair

H5: blue eyes



#### Prompt to test each hypotheses:

##### 1. H1\_black top:

['A woman with blonde hair wearing a black top', 'Blonde woman in a black top', 'A blonde female wearing a black top smiling', 'Portrait of a blonde woman wearing a black top', 'A young woman with blonde hair dressed in a black top']

##### 2. H2\_woman wearing a red dress:

['A woman with blonde hair wearing a red dress', 'Blonde woman in a red dress', 'A blonde female wearing a red dress smiling', 'Portrait of a blonde woman wearing a red dress', 'A young woman with blonde hair dressed in a red dress']

##### 3. H3\_blue dress:

['A woman with blonde hair wearing a blue dress', 'Blonde woman in a blue dress', 'A blonde female wearing a blue dress smiling', 'Portrait of a blonde woman wearing a blue dress', 'A young woman with blonde hair dressed in a blue dress']

##### 4. H4\_woman with long hair:

['A woman with blonde long hair', 'Blonde woman with long flowing hair', 'A blonde female with long hair', 'Portrait of a blonde woman with long hair', 'A young woman with long blonde hair']

##### 5. H5\_blue eyes:

['A woman with blonde hair and blue eyes', 'Blonde woman with blue eyes', 'A blonde female with blue eyes looking at the camera', 'Portrait of a blonde woman with blue eyes', 'A young woman with blonde hair and blue eyes']

Figure 21: LADDER discovers slices for biased attributes in RN Sup IN1k-based classifier for *blond* classification in *CelebA* dataset. This figure details the slice discovery process for biased attributes involving sentence analysis, hypothesis generation by an LLM, and the model's performance on slices where attributes are present or absent, demonstrating how biases affect classifier accuracy. We highlight the hypothesis generated by LADDER that corresponds to the ground truth biased attribute (e.g., woman for blond) in **yellow**.



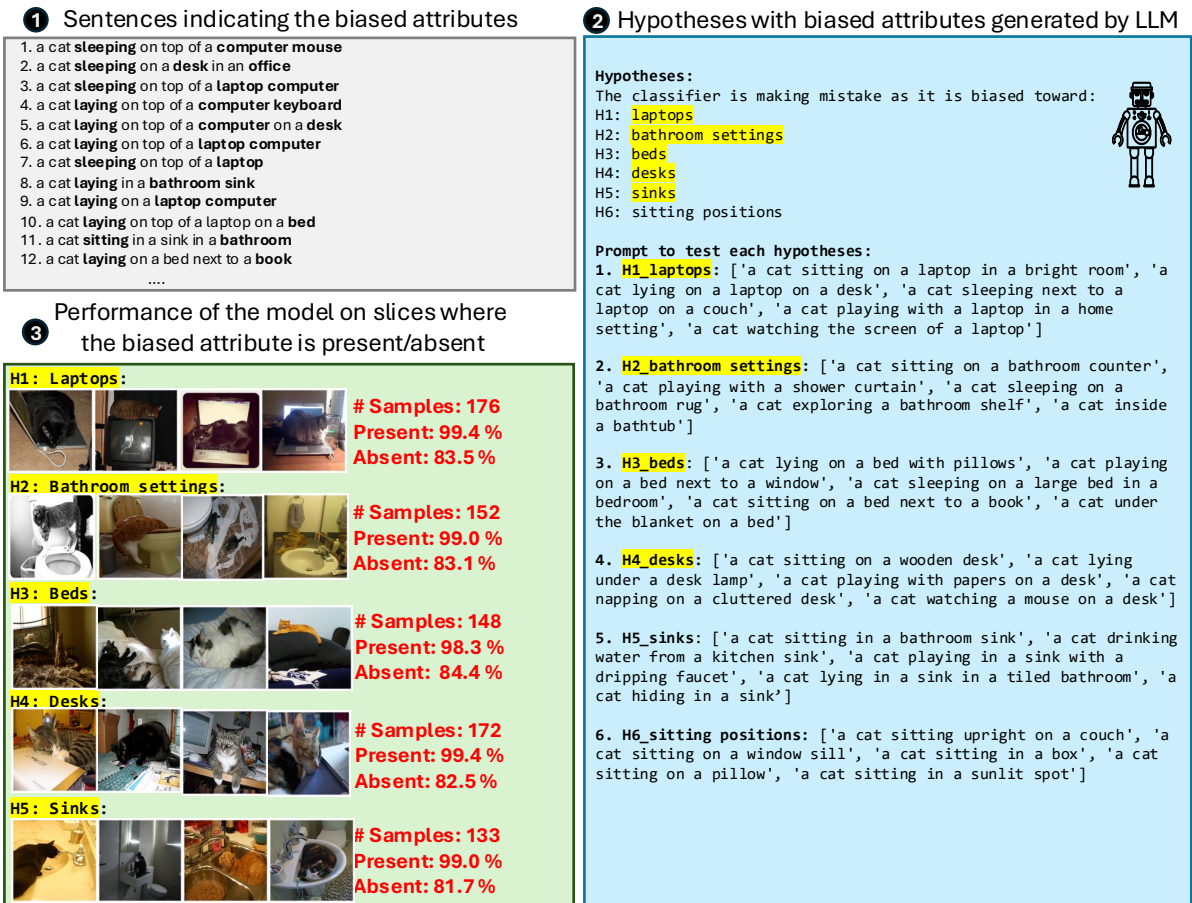


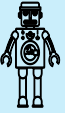
Figure 22: LADDER discovers slices for biased attributes in RN Sup IN1k-based classifier for *cat* classification in **MetaShift** dataset. This figure details the slice discovery process for biased attributes involving sentence analysis, hypothesis generation by an LLM, and the model’s performance on slices where attributes are present or absent, demonstrating how biases affect classifier accuracy. We highlight the hypothesis generated by LADDER that corresponds to the ground truth biased attribute (*e.g.*, indoor for cat) in **yellow**.

**1** Sentences indicating the biased attributes

1. a man walking a group of dogs on a **leash**
2. a group of people walking on the **beach** with their dogs
3. a dog playing in the water at the **beach**
4. a black and white dog playing with a toy in the **grass**
5. a dog is walking on the beach near the **water**
6. a group of men standing around a dog on a **leash**
7. a person walking a dog on a **leash**
8. a group of dogs playing in the **grass**
9. a dog walking on the **beach**
10. a woman **riding a surf board** with a dog
11. a man walking down the **street** holding a dog
12. a woman walking a dog on a **leash**
- ....

**2** Hypotheses with biased attributes generated by LLM

**Hypotheses:**  
 The classifier is making mistake as it is biased toward:  
 H1: objects related to sports, H2: **beach environments**,  
 H3: dogs in motion,  
 H4: dogs with objects in their mouths, H5:  
 dogs on leashes




**Prompt to test each hypotheses:**

1. **H1\_objects related to sports:** ['A dog sitting next to a tennis racket on a tennis court.', 'A dog running with a baseball bat in its mouth on a field.', 'A dog standing next to a basketball on a court.', 'A dog lying next to a soccer ball on a grass field.', 'A dog jumping to catch a frisbee in a park.']
2. **H2\_beach environments:** ['A dog running on the beach near the ocean.', 'A dog playing in the sand at the beach.', 'A dog standing on a surfboard in the water.', 'A dog and a person walking along the shore of a beach.', 'A dog digging a hole in the sand at the beach.']
3. **H3\_dogs in motion:** ['A dog running rapidly in a field chasing a ball.', 'A dog jumping over a hurdle in an agility course.', 'A dog chasing its tail in a park.', 'A dog sprinting along a street next to a moving car.', 'A dog leaping into a pond to fetch a stick.']
4. **H4\_dogs with objects in their mouths:** ['A dog carrying a newspaper in its mouth coming towards the porch.', 'A dog holding a frisbee in its mouth ready to play.', 'A dog fetching a stick in its mouth from the water.', 'A dog with a slipper in its mouth greeting its owner.', 'A dog carrying a ball in its mouth during a walk in the park.']
5. **H5\_dogs on leashes:** ['A person walking a dog on a leash down a busy street.', 'A dog on a leash sitting patiently at a bus stop.', 'A dog on a leash interacting with another dog in a park.', 'A dog on a leash being trained by its owner in obedience class.', 'A dog on a leash waiting outside a store while its owner shops.']


**3** Performance of the model on slices where the biased attribute is present/absent

**H1: Objects related to sports:**




**# Samples: 133**  
**Present: 98.0 %**  
**Absent: 84.9 %**

**H2: Beach environments:**




**# Samples: 128**  
**Present: 99.4 %**  
**Absent: 82.1 %**

**H3: Dogs in motion:**




**# Samples: 116**  
**Present: 99.4 %**  
**Absent: 82.4 %**

**H4: Dogs with objects in their mouths:**



**# Samples: 109**  
**Present: 99.2 %**  
**Absent: 82.2 %**

**H5: Dogs on leashes :**



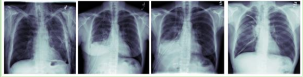




**# Samples: 125**  
**Present: 99.2 %**  
**Absent: 81.7 %**

Figure 23: LADDER discovers slices for biased attributes in RN Sup IN1k-based classifier for *dog* classification in **MetaShift** dataset. This figure details the slice discovery process for biased attributes involving sentence analysis, hypothesis generation by an LLM, and the model’s performance on slices where attributes are present or absent, demonstrating how biases affect classifier accuracy. We highlight the hypothesis generated by LADDER that corresponds to the ground truth biased attribute (e.g., outdoor for cat) in **yellow**.

### 1 Sentences indicating the biased attributes

1. perhaps mild **increase** in **hydropneumothorax** but with **chest tube** remaining in place and no striking change
2. in comparison with the study of \_\_\_\_, there is little change in the **3 left chest tubes** with area of **hydro pneumothorax** persisting in the lateral aspect of the **upper left chest** as well as probably the left lung base
3. a **moderate sized loculated hydropneumothorax** shows decrease in **fluid** component and increasing gas component, particularly in the **right base**
4. small **right** pleural effusion has replaced the previous **basal pneumothorax** that developed with previous drainage of pleural effusion and placement of **2 thoracostomy tubes**
5. **2 right** indwelling **pleural drains** are unchanged in their **respective positions**, and there has probably been some decrease in the volume of the **right posterior air** and pleural collection in the rib **right lower hemi thorax**

### 3 Performance of the model on slices where the biased attribute is present/absent

<b>H1: Loculated characteristics of pneumothorax:</b>	
	<b>Present: 87.0 %</b> <b>Absent: 28.3 %</b>
<b>H2: presence of chest tubes:</b>	
	<b>Present: 97.7 %</b> <b>Absent: 31.1 %</b>
<b>H3: Fluid levels in pneumothorax:</b>	
	<b>Present: 88.2 %</b> <b>Absent: 48.3 %</b>
<b>H4: size and extent descriptions of pneumothorax:</b>	
	<b>Present: 86.4 %</b> <b>Absent: 49.8 %</b>
<b>H5: side of the body affected by pneumothorax:</b>	
	<b>Present: 87.2 %</b> <b>Absent: 48.7 %</b>

### 2 Hypotheses with biased attributes generated by LLM

#### Hypotheses:

The classifier is making mistake as it is biased toward:

- H1: loculated characteristics of pneumothorax
- H2: presence of **chest tubes**
- H3: fluid levels in pneumothorax
- H4: size and extent descriptions of pneumothorax
- H5: side of the body affected by pneumothorax



#### Prompt to test each hypotheses:

##### 1. H1\_loculated characteristics of pneumothorax:

['Chest X-ray showing loculated pneumothorax with varying air and fluid levels', 'Loculated air pockets in pneumothorax as seen in a chest radiograph', 'Pneumothorax with loculated air collections complicating the diagnosis', 'Loculated pneumothorax with complex air and fluid separation', 'Detailed view of loculated pneumothorax with chest tube intervention']

##### 2. H2\_presence of chest tubes:

['Chest X-ray with visible chest tubes in place for pneumothorax treatment', 'Pneumothorax management with chest tubes as seen in the radiograph', 'Chest radiograph depicting the placement of chest tubes in pneumothorax', 'Influence of chest tubes on the appearance of pneumothorax in X-ray images', 'Chest tubes in situ for a patient with pneumothorax on the radiograph']

##### 3. H3\_fluid levels in pneumothorax:

['Chest X-ray showing pneumothorax with significant fluid levels', 'Pneumothorax with varying degrees of fluid accumulation in chest X-ray', 'Radiographic appearance of pneumothorax with fluid levels', 'Assessment of fluid levels in pneumothorax via chest radiography', 'Fluid levels indicating severity of pneumothorax in a chest X-ray']

##### 4. H4\_size and extent descriptions of pneumothorax:

['Chest X-ray showing a large pneumothorax covering extensive lung area', 'Moderate sized pneumothorax visible on the right side in chest X-ray', 'Small apical pneumothorax detected in a routine chest X-ray', 'Extent of pneumothorax as a critical factor in chest X-ray analysis', 'Evaluating the size and spread of pneumothorax in chest radiographs']

##### 5. H5\_side of the body affected by pneumothorax:

['Right-sided pneumothorax as shown in chest X-ray imaging', 'Left basal pneumothorax detected in a diagnostic chest X-ray', 'Chest X-ray revealing pneumothorax on the left side of the chest', 'Comparison of right and left side pneumothorax in X-ray images', 'Implications of pneumothorax location on the left side in chest X-rays']

Figure 24: LADDER discovers slices for biased attributes in RN Sup IN1k-based classifier for *pneumothorax* classification in **NIH-CXR** dataset. This figure details the slice discovery process for biased attributes involving sentence analysis, hypothesis generation by an LLM, and the model's performance on slices where attributes are present or absent, demonstrating how biases affect classifier accuracy. We highlight the hypothesis generated by LADDER that corresponds to the ground truth biased attribute (e.g., chest-tube for landbirds) in **yellow**.

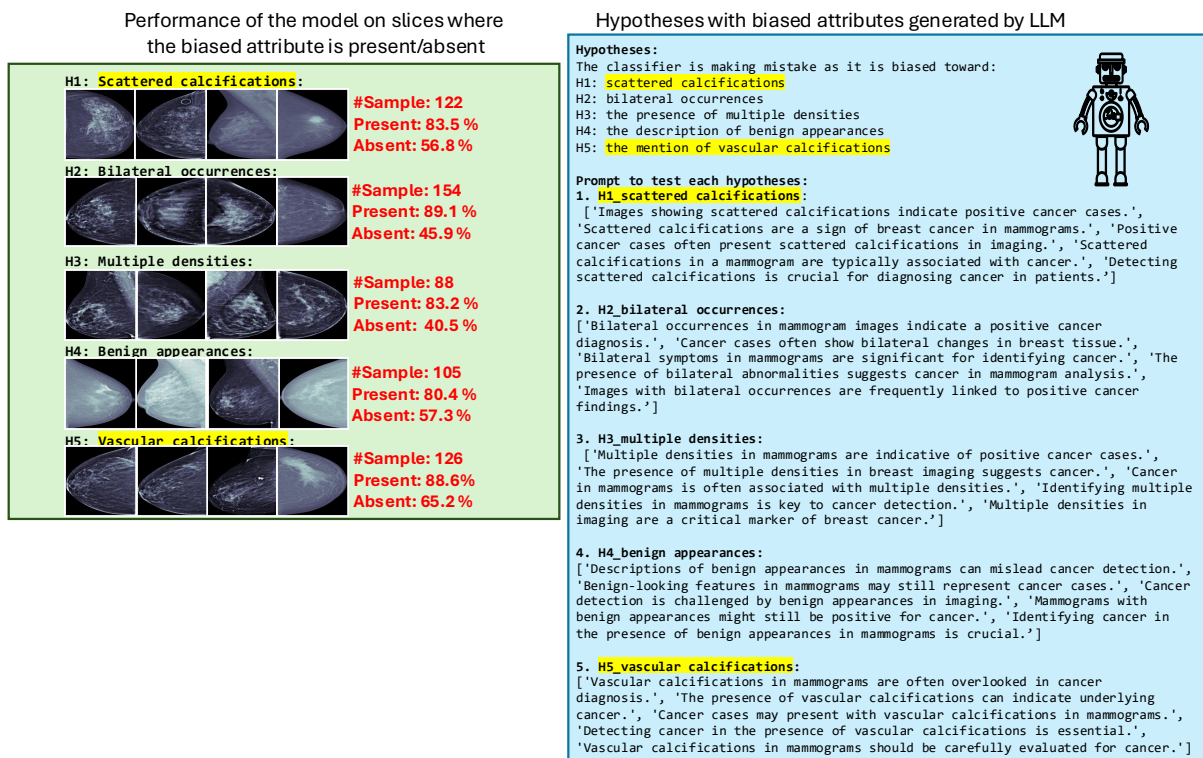


Figure 25: LADDER discovers slices for biased attributes for *cancer* classification in **RSNA-Mammo** dataset. This figure details the slice discovery process for biased attributes involving sentence analysis, hypothesis generation by an LLM, and the model's performance on slices where attributes are present or absent, demonstrating how biases affect classifier accuracy. We highlight the hypothesis generated by LADDER that corresponds to the ground truth biased attribute (e.g., calcification for cancer) in **yellow**.